Sensitivity of subglacial drainage to water supply distribution at the Kongsfjord basin, Svalbard

Chloé Scholzen[1], Thomas V. Schuler[1], Adrien Gilbert[2]

[1]Department of Geosciences, University of Oslo, Norway
5 [2]Université Grenoble-Alpes, CNRS, IGE, Grenoble, France

Correspondence to: Chloé Scholzen (chloe.scholzen@geo.uio.no)

Abstract. By regulating the amount, the timing and the location of meltwater supply to the glacier bed, supraglacial hydrology potentially exerts a major control on the evolution of the subglacial drainage system, which in turn modulates sliding. Yet the configuration of the supraglacial hydrological system has received only little attention in numerical models

10 of subglacial hydrology so far. Here we apply the ~~two dimensional~~ two-dimensional subglacial hydrology model GlaDS to a Svalbard glacier basin with the aim of investigating how the spatial distribution of meltwater recharge affects the characteristics of the basal drainage system. We design four experiments with various degrees of complexity in the way that meltwater is delivered to the subglacial drainage model. Our results show significant differences between experiments in the early-summer transition from distributed to channelized drainage, with discrete recharge at moulins favouring channelization

15 ~~and driving earlier rise in basal water pressure~~ at higher elevations and driving overall lower water pressures. Otherwise, we find that water input configuration only poorly influences subglacial hydrology, which is controlled primarily by subglacial topography. All experiments fail to develop channels of sufficient efficiency to substantially reduce summertime water pressures, which we impute to small surface gradients and short melt seasons. The findings of our study may be extended to most Svalbard tidewater glaciers with similar topography and low meltwater recharge. The absence of efficient

20 channelization implies that the dynamics of tidewater glaciers in the Svalbard archipelago may be sensitive to future long-term trends in meltwater supply.

1 Introduction

Land-based ice masses, as they undergo rapid change due to climate warming, are one of the largest potential contributors to global sea level rise (AMAP, 2017; Pörtner et al., 2019; Wouters et al., 2019). Regional glacier change also affects surface

25 albedo, coastal ecology, as well as hydrological management in terms of flood hazards, hydropower and freshwater supply (Vincent et al., 2011; Fountain et al., 2012; Carey et al., 2017; Milner et al., 2017). As such, predicting and adapting to future alterations in the glacial landscape relies on better understanding glacier response to changing climate. Field observations and modelling experiments suggest that, besides increasing mass loss, higher meltwater production may also alter ice dynamics (Hewitt, 2013; Gagliardini and Werder, 2018; Davison et al., 2019). Seasonal ice flow accelerations following

30 periods of enhanced surface melt have been reported for glaciers worldwide (e.g. Iken et al., 1983; Mair et al., 2001; Zwally et al., 2002; Copland et al., 2003), including polythermal glaciers in Svalbard (Dunse et al. 2012, 2015; Schellenberger et al., 2015). On shorter timescales (i.e. hourly or daily), episodic speedups have been found concurrent with intense melting, heavy rainfall, and supraglacial lake drainage (e.g. Joughin et al., 2013; Horgan et al., 2015).

Both theoretical and observational studies have long established that meltwater reaching the glacier bed modulates basal

35 water pressure, which in turn affects ice motion through basal sliding (e.g. Lliboutry, 1968; Bindschadler, 1983; Iken and Bindschadler, 1986; Sugiyama and Gudmundsson, 2004). The relationship between water input and sliding is nevertheless complicated by the morphology of the subglacial hydrological system (Bartholomew et al., 2010; Sole et al., 2011; Sundal et al., 2011; Cowton et al., 2013). High basal water pressures and acceleration are typically related to subglacial flow in distributed linked cavities (inefficient drainage) (Kamb, 1987; Iken and Truffe, 1997), whereas lower water pressures and ice

40 flow deceleration are imputed to channelization (efficient drainage) (Röthlisberger, 1972; Nienow et al., 1998; Schoof, 2010).

Hydrological processes taking place inside and below glaciers are of substantial complexity and remain poorly understood due to the sparsity of direct observations. To address this lack of knowledge, numerous modelling approaches have been developed in the past decades, with much of the recent effort directed at the coupling between glacier dynamics

45 and basal water pressure (e.g. Schoof, 2010; Hewitt, 2013; de Fleurian et al., 2014; Hoffman and Price, 2014; Bueler and Van Pelt, 2015). However, so far only a handful of these studies have focused on the role of supraglacial hydrology in the evolution of the subglacial drainage system (Clason et al., 2015; Wyatt et al., 2015; Banwell et al., 2016; Koziol et al., 2017; Decaux et al., 2019). As pointed out by Flowers (2015), most conceptual models of subglacial hydrology implicitly assume that recharge of surface water to the glacier bed is homogeneous (e.g. Flowers and Clarke, 2002; Hewitt, 2011; Pimentel and

50 Flowers, 2011). In nature, water supply to the subglacial environment is rarely uniform and usually collects meltwater produced in an upstream area of the glacier surface. In the accumulation zone, recharge to the bed is delayed as the surface-generated water percolates through the snow and firn pack, where some fraction may be temporarily retained as slush, or may refreeze if subsurface temperatures are below melting point (Pfeffer et al., 1991; Van Pelt et al., 2016). The water that escapes the firn is conveyed by englacial conduits to the subglacial system (Gulley et al., 2009a, 2009b; Benn and Evans,

55 2010). In the bare-ice zone, surface meltwater collects in supraglacial streams and is routed downglacier over hundreds of meters to several kilometres. Within one melt season, surface meltwater either enters a crevasse, a moulin or a supraglacial lake, or leaves the glacier by running off the glacier edge. Both crevasses and moulins are important surface-to-bed hydrological connections as they can be found over the entire glacier. Moulins are near-vertical conduits that result from water pouring into a crevasse and melt-enlarging it through frictional heating. As they are typically fed by supraglacial

60 streams, moulins capture runoff from upstream watersheds. By transferring significant volumes of water to the glacier bed at discrete points, moulins can initiate channels in subglacial regions that may not be predicted by simple hydrological models which use the minimum hydraulic potential pathway minimum to determine channel locations (Gulley et al., 2012). Moulins persist over multiple years if they receive frequent water delivery from the supraglacial system, and therefore may have a

long-lived impact on the subglacial hydrology (Catania and Neumann, 2010). Consequently, explicit representation of water
recharge to the base of glaciers may be crucial to accurately simulate how the subglacial hydrological system, and hence ice
dynamics, respond to increased meltwater production and variability in a warming climate.

Here we apply a two-dimensional ~~distributed~~ model of subglacial hydrology (GlaDS) (Werder et al., 2013) to a Svalbard
polythermal glacier basin. The model, which couples distributed and channelized drainage, is forced with distributed supply
rates from a calibrated surface-energy-balance-snow model (Van Pelt et al., 2019). We define different water input
configurations that include spatially continuous and/or discrete subglacial water recharge with aims to: (a) investigate how
approximations ~~on~~ about water supply to the bed affect the development of the modelled subglacial hydrological system, and
(b) describe the basal drainage system at the Kongsfjord basin, with special focus on basal water pressure distribution,
drainage efficiency, and its implications for glacier sliding.

2 Study area

2.1 Glaciers and topography

The Kongsfjord basin, located in northwestern Svalbard, covers a total land area of approximately 1,430 km^2, of which about
75 % is glacierised. The basin surrounds Kongsfjorden, which stretches over ~20 km towards the Arctic Ocean to the west.
This study centers on three adjacent glacier systems that terminate in the inner part of Kongsfjorden (Fig. 1(a)):
Isachsenfonna/Kongsbreen, Holtedahlfonna-Infantfonna/Kronebreen, and Kongsvegen.

At the northeastern fjord head, the ice field Isachsenfonna drains through the outlet glacier Kongsbreen (together 378
km^2), which splits due to a bedrock ridge into two branches, Kongsbreen North and Kongsbreen South. To the east, the
terminal glacier Kronebreen is fed by two contributory catchments: the larger ice field Holtedahlfonna and the smaller
Infantfonna (together 373 km^2). Roughly 5 km from its front, Kronebreen is confluent with Kongsvegen (108 km^2), and the
two glacier tongues share a common terminus which is currently dominated by Kronebreen (Sund et al., 2011).

Surface elevation (Fig. 1(a)), basal topography (Fig. 1(b)), and ice thickness of the Kongsfjord basin were recently
mapped by airborne and ground-based ice-penetrating radar (Lindbäck et al., 2018). Together with their accumulation areas,
the Kongsfjord glaciers span an altitudinal range from sea level to 1,400 m a.s.l. in the northern parts of their catchments
(Fig. 1(a)). Below the equilibrium line altitude, which for Holtedahlfonna/Kronebreen was estimated around 610 m a.s.l. for
the period 1961–2012 (Van Pelt and Kohler, 2015), Kronebreen is heavily crevassed and its slope is disrupted by several ice
falls. In the ablation area, the subglacial topography is characterised by extended troughs as deep as −180 m a.s.l. under
Kongsbreen North, −130 m a.s.l. under Kronebreen, and −70 m a.s.l. under Kongsvegen (Fig. 1(b)). Both Kronebreen and
Kongsvegen are fully grounded below sea level over their lowermost 10 km and 9 km, respectively, whereas Kongsbreen
South is mostly resting on bedrock above the water line. A few nunataks peak through the lower parts of the glaciers at

approximately 500–600 m a.s.l.. Further inland, the subglacial topography smoothens into wide flat valleys around 200 m
95   a.s.l., and ice thickens with a maximum of 740 m in the middle of Isachsenfonna.

2.2 Mass balance and dynamics

Like most tidewater glaciers in Svalbard, the Kongsfjord glaciers have a negative mass balance dominated by calving, a finding that both in situ measurements and modelling experiments have corroborated over the last decades (e.g. Lefauconnier et al., 1994b; Nuth et al., 2012). More recently, Van Pelt and Kohler (2015) used a coupled surface-energy-balance—snow
100 model to include superimposed ice and internal accumulation in their surface mass balance calculations. For Kronebreen and Kongsvegen, they found that surface mass balance is controlled by mass gain through precipitation (0.87 m w.e. a^{-1}) and mass loss through runoff (0.79 m w.e. a^{-1}), and that refreezing of water in the firn layer (0.30 m w.e. a^{-1}) provides a strong buffer for runoff. Their results also reveal a 31 % increase in runoff since 2000, coinciding with higher surface melt rates and lower refreezing rates in response to recent warming and firn line retreat.

105   Kronebreen is one of the fastest-flowing glaciers in Svalbard (Liestøl, 1988; Sund et al., 2011). Near the terminus, mean annual surface velocities are persistently high (1.6–2.15 to m day^{-1}) (Lefauconnier, 1987; Lefauconnier et al., 1994a; Kääb et al., 2005), and summer velocities peak up to 3.2 m day^{-1} (Schellenberger et al., 2015). Such high velocities can only be achieved through basal sliding, which indicates that the glacier base is temperate. Kongsbreen has a more complex velocity pattern, due to its split into two separate terminal branches: the northern, marine-terminating branch of the glacier is fast-
110 flowing, with a maximal speed of 2.7 m day^{-1} measured in 2012 (Schellenberger et al., 2015), whereas the southern, partially land-terminating branch is slow-moving. Both Kronebreen and Kongsbreen North exhibit clear seasonal flow variability characterised by relatively stable and low velocities in autumn and winter, and an acceleration synchronous with the melt season. Schellenberger et al. (2015) observed that, at both glaciers, a large part of the ice flow variability followed fluctuations in surface meltwater production and rainfall, a correlation that they attributed to variations in basal lubrication.
115 Evidence from later studies also strongly suggest that multiannual changes in ice flow at Kronebreen are controlled by changes in the subglacial hydrology (How et al., 2017; Vallot et al., 2017). Interannual variability in ice velocity as well as upglacier propagation of seasonal speedup were both found to be higher at Kronebreen than at Kongsbreen North (Schellenberger et al., 2015), indicating different basal conditions at the two glaciers. Kongsvegen, a surge-type glacier that is currently in its quiescent phase, contrasts with the other Kongsfjord glaciers in its dynamics. Since its last surge in 1948
120 (Melvold and Hagen, 1998), the glacier has experienced very little motion (2–8 m a^{-1}), negligible calving and significant surface steepening (Hagen et al., 1999; 2005; Nuth et al., 2012).

2.3 Subglacial hydrology

Glaciers in Kongsfjord are polythermal, usually with basal temperatures at or close to the pressure melting point, meaning that water drains at their base all year through (Björnsson et al., 1996; Sevestre et al., 2015; Nuth et al., 2019). Glacial runoff is periodically released into the fjord, where it produces sediment-rich freshwater plumes that are of great importance for the glacio-marine dynamics and the ecosystem of Kongsfjorden (Svendsen et al., 2002; Everett et al., 2018).

In recent years, several locations of subglacial discharge have been identified at the Kronebreen-Kongsvegen terminal complex: one main outlet in the northern half of the glacier tongue, and several secondary outlets near the Kronebreen-Kongsvegen junction (Trusel et al., 2010; Kehrl et al., 2011; Everett et al., 2018). Contrasts in plume timing and duration have been suggested to reflect local differences in subglacial drainage efficiency across glacier termini (Schild et al., 2016; Slater et al., 2017). How et al. (2017) monitored plumes at Kronebreen and combined the data with observations of borehole water pressure, supraglacial lake drainage, surface velocities, as well as modelling of meltwater routing, to infer the morphology of the subglacial hydrological system during summer 2014. Their results indicated that meltwater was largely drained to the northern part of the terminus through a channelized system connected to the upper catchment area (Holtedahlfonna), hence the broader and more persistent plume on the northern side. By contrast, the intermittent activity of the southern plume during the 2014 melt season was attributed to distributed drainage of a smaller catchment area.

Spatiotemporal variations in basal properties at Kronebreen were also investigated by Vallot et al. (2017) through inverting surface velocities for 2013–2015 to determine a basal friction coefficient. Their modelling results supported conclusions drawn by the earlier studies, i.e. that subglacial hydrology organisation is as much a key factor to basal sliding as are local characteristics such as bed topography and summer melt.

While the relationship between meltwater supply, subglacial hydrology and ice velocity is well documented at Kronebreen (Schellenberger et al., 2015; How et al., 2017), similar knowledge is lacking at the neighbouring outlet glaciers (Kongsvegen, Kongsbreen North and Kongsbreen South), and the subglacial hydrology at the upper ice fields (Isachsenfonna, Holtedahlfonna and Infantfonna) remains yet to be examined.

3 Methods and datasets

3.1 Mapping of supraglacial hydrology

Mapping of Kongsfjord's supraglacial drainage system is achieved using TopoToolbox, a collection of scripts to analyse flow pattern in digital elevation models (DEMs) (Schwanghart and Scherler 2014). TopoToolbox first seeks to determine surficial water movement within the DEM. Flow direction calculation is based on a ~~multiple~~ single flow direction algorithm that examines elevation gradients between grid cells. ~~The multiple flow direction algorithm allows for both convergence and divergence of flow, thus producing more realistic flow pathways than the single flow direction algorithm.~~ Next, information

on flow direction is used to derive: (1) flow accumulation, i.e. the number of cells draining in each grid cell, (2) the drainage network, i.e. the estimated flow paths in the DEM, and (3) drainage basins, i.e. the upslope areas contributing to each grid cell in the drainage network. We generate a map of the supraglacial stream network, shown in Fig. 2(c), and the watersheds associated to each moulin (Fig. 2(c,d)). The selection of the moulin locations is described in Sect. 3.3.2.

3.2 Modelling of subglacial hydrology

To simulate the subglacial hydrology of the Kongsfjord basin, we employ the Glacier Drainage System model (GlaDS) (Werder et al., 2013), a ~~distributed~~ two-dimensional model developed to describe subglacial water drainage and ~~that~~ which participated in the Subglacial Hydrology Model Intercomparison Project (SHMIP) (de Fleurian et al., 2018). GlaDS has been implemented in Elmer/Ice, an open source, finite-element model (Gagliardini et al., 2013), which in this study serves only as platform for the subglacial hydrology model. The implementation of GlaDS in Elmer/Ice is detailed in Gagliardini and Werder (2018).

The subglacial hydrology model GlaDS accounts for both inefficient distributed drainage and efficient channelized drainage to compute the evolution of the hydraulic potential at the glacier base. The distributed network of linked cavities is featured in the form of a continuous water sheet across the model domain, which is fed by a source term at each node on the mesh. We define the source term from the sum of a space and time varying surface water input, as described in Sect. 3.4.2, and a uniform, steady basal melting. Discrete channels that form on the edges of the mesh elements constitute the efficient drainage system. Between each pair of nodes, channel segments develop from water exchange with the adjacent sheet as well as from water input at moulins, which act as local sources. Moulins are shaped as vertical cylinders at some of the mesh nodes (see Sect. 3.3.2), and deliver water directly from the glacier surface to the basal channel network. Depending on their cross-sectional area and on the subglacial water pressure, moulins can store a certain volume of water, as revealed by tracer-experiments (Werder and Schuler, 2010). For a complete description of the equations solved by the GlaDS model, we redirect readers to Werder et al. (2013).

The problem is solved on a mesh constructed by discretising the domain using irregular triangulation with a mean edge length of 250 m, which yields 11,824 nodes in total. The mesh resolution is a compromise between numerical computation time and spatial precision of the model outputs. To ensure computational stability, the simulation time step does not exceed 1 day, and adaptive time stepping down to ~1.5 minutes is applied. Additional gain of computation time is achieved through partitioning and parallel simulation of each model run.

As boundary conditions, channels are not allowed to develop along the outer limits of the model domain, and the hydraulic potential is set to zero at the glacier fronts because we consider that all three termini (Kongsbreen North, Kongsbreen South, and Kronebreen-Kongsvegen) are freely connected to the fjord~~, which imposes the water pressure~~. Indeed, by imposing the water pressure to be equal to sea pressure at the depth of at the outlets, we have

$$\varphi = \varphi_m + p_w = \rho_w g z_b + \rho_w g (z_{sl} - z_b) = 0$$

where φ is the hydraulic potential, φ_m the elevation potential, p_w the sea water pressure, z_b the bed elevation, and z_{sl} the sea level elevation (= 0 m a.s.l.).

The values for the model parameters are set out in Table 1. The grey highlighted parameters are those to which we assigned values different from the literature. We adapted values for conductivity parameters as well as for sheet width below channel to facilitate channelization and to maximise the influence of meltwater input on the subglacial drainage efficiency. More specifically, our value for the sheet conductivity is lower than the one originally proposed by Werder et al. (2013), but inspection of current literature revealed that others find better agreement to observations by using lower values (e.g. Dow et al., 2018; Dow et al., 2020) or even suggest a seasonally variable conductivity (Downs et al., 2018). We performed sensitivity tests and found that lower sheet conductivities lead to higher water pressures all year round, whereas the original value from Werder et al. (2013) yields unrealistically low water pressures in winter. We also found our model results to be largely insensitive to changes in channel conductivity. In addition, we set a uniform basal sliding speed of ~315 m a^{-1} (10^{-5} m s^{-1}) for the entire domain, which corresponds roughly to the glacier-averaged surface speed measured by satellite imagery in the Kongsfjord basin (Schellenberger et al., 2015).

3.3 Water supply to the subglacial drainage system

In order to investigate the sensitivity of our subglacial hydrology model to water recharge distribution, we design four model experiments with various degrees of complexity in the way that water is delivered to the glacier beds. The control experiment is the simplest scenario, in which basal water supply is spatially continuous and identical to surface meltwater production. The next two experiments assume discrete water recharge to the basal drainage system through moulins, with the latter including only water that is drained in moulins catchments. Finally, the fourth and most realistic scenario builds upon local knowledge of glacial hydrology at Kongsfjord. This experiment accounts for immediate surface-to-base water transfer via crevasses in the ablation zone, as well as for catchment-wide water collection into moulins in the accumulation zone. Water input is taken from a raster of modelled recharge values, as described in Sect. 3.4.2 below.

3.3.1 Experiment 1

In the first experiment, the gridded water input is interpolated to every mesh node of the GlaDS model and is directly injected into the distributed sheet layer, regardless of the supraglacial hydrology (Fig. 2(a)). This approximation is ~~most~~ still commonly made in subglacial hydrology models, based on the assumption that glaciers are perfectly 'permeable' in that they allow meltwater to travel straight from their surface to their beds (e.g. Cook et al., 2020). We use this experiment as a reference against which we compare the other experiments with the aim of assessing the effect of adding complexity to water supply distribution.

3.3.2 Experiment 2

In this scenario, water input is restricted to only a few moulins that act as individual sinkholes at the glacier surface. We evenly redistribute the total recharge between the moulins, so that at each time step every moulin receives the same amount of water. We consider 13 moulins in total, five of which have been previously identified as active supraglacial lakes that drained to the glacier base at least once between 2014 and 2017. ~~In addition, based~~ The other eight moulins are manually detected on high-resolution aerial images derived from TopoSvalbard (https://toposvalbard.npolar.no/, Norwegian Polar Institute)~~, we manually detect at least 20 more moulins, of which we keep only 10 that are in vicinity to the supraglacial stream network inferred by TopoToolbox (Fig. 2(c))~~. Each moulin is then defined at the closest mesh node of the model domain. All 13 moulins are located between approximately 3–35 km from the glacier termini, and at surface elevations between 400 and 700 m a.s.l. (Fig. 2(b)). Except for Kongsvegen, we do not detect any moulin in the lower parts of the other glaciers since these areas are highly crevassed. Both the location and the cross-sectional area (see Table 1) of the moulins are assumed constant over the study period.

3.3.3 Experiment 3

Here we impose discrete water input at the same 13 moulins as in Experiment 2, with the difference that water recharge is calculated from the upstream catchment area that is associated to each moulin (Fig. 2(c)). Meltwater produced downstream of moulins is not taken into account in this scenario. Using the TopoToolbox program (described in Sect. 3.1 above), we delineate the supraglacial watersheds and retrieve the meltwater volume in each of them. The moulins catchments are assumed to remain stationary over the study period. The total water amount involved here is slightly higher than in Experiments 1–2 because this scenario accounts for meltwater in watersheds that extend beyond the glacier boundaries.

3.3.4 Experiment 4

Finally, we develop an experiment in which we attempt to describe as realistically as possible the spatial distribution of water supply to the glacier beds. Here, we combine continuous and discrete recharge to the subglacial hydrological system. In crevassed areas of the Kongsfjord basin, we apply direct surface-to-bed transfer of meltwater into the sheet layer, in the same fashion as for Experiment 1. The crevassed zones are manually mapped on 1 m resolution satellite images from Pleiades (© CNES (2014), and Airbus DS (2014), all rights reserved. Commercial uses forbidden). It should be noted that, whilst some minor cracks are also detected in Holtedahlfonna and Isachsenfonna, the extent of these crevassed areas is probably underestimated because of the snow cover. In the higher parts of the domain, we adapt the configuration of Experiment 3 by including only the moulins that are located in non-crevassed areas. In addition, we consider six new moulins, which raises the total number of moulins to 19. These moulins were identified from Fig. 2(c), wherever a supraglacial stream crosses the upper boundary of a crevassed area. The moulin catchments are adjusted as well in order to

accommodate the additional moulins, and to exclude the crevassed areas where water drains directly into the subglacial system and does not contribute to the moulin discharge (Fig. 2(d)).

3.4 Datasets

3.4.1 Study area outline and topography

The TopoToolbox analysis is carried out on a 40 m resolution DEM acquired in 2007 from the SPOT-5 satellite sensor (Bouillon et al., 2006; Korona et al., 2009). Kongsfjord's glacier outlines of 2007 are retrieved from the Randolph Glacier Inventory (König et al., 2013) and are used to shape the model domain. Basal topography is taken from a 150 m resolution DEM produced by Lindbäck et al. (2018). The glacier outlines are adjusted to avoid zero (and occasionally occurring negative) ice thickness, which would compromise model calculations. Inside the modelled glacier basin, nunataks are also cut out. This model domain, which covers a total surface area of 519 km^2, is used for all model runs in this study.

3.4.2 Water input

Water supply to the subglacial hydrological system is derived from a surface runoff time series generated by a coupled surface-energy-balance - snow model that uses downscaled output from the regional climate model HIRLAM as atmospheric forcing (Van Pelt and Kohler, 2015; Van Pelt et al., 2019). The model accounts for subsurface processes such as water storage in the porous firn layer, as well as refreezing/melting of water in the snowpack. Here recharge is the liquid water volume that effectively reaches the glacier bed. More specifically, in the accumulation zone recharge is the amount of liquid water available at the firn-ice transition, which is the sum of percolated rain and surface-generated meltwater minus the water that is retained in the snow and firn pack (Van Pelt et al., 2016). In the case of bare-ice exposure, such as in the ablation zone during summertime, recharge is the sum of rain and meltwater at the ice surface. The time series covers the period 2004̶3̶ to 2017 with a 3 hourly time step (subsequently averaged to the 1 day simulation time step) and a 1 km grid resolution.

4 Results and analysis

Each Glacier Drainage System model run consisted of a 1-year spin-up and a ̶1̶5̶ ̶y̶e̶a̶r̶ 14-year simulation period with one of the four water input configurations described in the previous section. For each model run, we examine the subglacial water pressure (expressed as a fraction of the ice overburden pressure), the water flux in the distributed drainage system (sheet flux) as well as in the channelized drainage system (channel flux), and the absolute value of hydraulic head. We explore the mean seasonal variation of these variables both over the entire glacier basin and at three cross-glacier transects (indicated in Fig. 1(b)). We also study the spatial distribution of these variables over the whole model domain, as well as along five

subglacial flowlines (indicated in Fig. 1(b)). To investigate differences in the subglacial hydrology between the model experiments, we use the simplest scenario (Experiment 1) as a reference against which we compare the other three water input configurations. Finally, we use the most realistic scenario (Experiment 4) to describe the mean spatiotemporal evolution of the subglacial hydrology at the Kongsfjord basin over the study period.

4.1 Comparison between experiments

4.1.1 Water input

Between 20~~04~~3 and 2017, the modelled average melt season lasts approximately from the 1st of June to the 30th of September in all experiments (Fig. 3(a)). In general, despite strong interannual variability, the mean peak in water supply occurs at the end of July. However, input water volumes vary among the four experiments due to different sizes of water contributing surface area. In Experiments 1–2, the same total water volume (~~1.57 × 10⁶ m³ day⁻¹~~2.96 × 10³ km³ over 20~~04~~3–2017) is supplied to the bed because recharge is calculated from the same surface area in both configurations (Fig. 2(a, b)). Experiments 3–4 deliver overall larger water volumes to the bed (~~1.76 × 10⁶ m³ day⁻¹~~3.32 × 10³ km³, and ~~2.55 × 10⁶ m³ day⁻¹~~3.44 × 10³ km³, respectively, over 20~~04~~3–2017) than Experiments 1–2 since these scenarios include supraglacial catchments that extend beyond the glacier boundaries (Fig. 2(c, d)). In Experiment 3, the early-summer increase in water input is slightly delayed compared to the other configurations because this scenario accounts for meltwater only in the higher parts of the glaciers (as described in Sect. 3.3.3 above), where surface melting starts later than at lower elevations.

4.1.2 Subglacial water pressure

All model experiments exhibit a similar seasonality in responses of the subglacial hydrology (Fig. 3(b)). Each water supply scenario rapidly raises the domain-averaged basal water pressure in the early melt season (June–July), followed by a much slower decline ~~starting at the end of July and~~ lasting through the subsequent winter (Fig. 3(b)). The minimum in water pressure occurs just before the onset of the next melt season. Despite the positive relation between water input and basal pressure on the seasonal scale, the water pressure signal appears smoother than that of the water input on daily timescale, showing less short-term variability. ~~The lowest short term variability in water pressure is found in the reference scenario (Experiment 1), reflecting a more distributed water input leading to lower amplitude in water pressure fluctuations.~~

Varying the water input configuration has minimal impact on the wintertime subglacial water pressure (Fig. 4(a–d)), since surface meltwater production outside of the melt season is close to zero. In all four scenarios, mean wintertime water pressure settles between ~55–60 % of the ice overburden pressure, with only Experiment 1 reaching up to 60 %. Sensitivity to the water input configuration is highest ~~at the start~~ during the first half of the melt season (June~~,~~–July)~~, when pressure builds up from low winter levels~~ when meltwater inputs differ most between the scenarios and pressure builds up from lower winter levels. Experiment 2 drives the earliest ~~sharpest~~ increase in basal pressure, followed by Experiments 1–4–3 ~~4 1 3~~, but peaks lower (~80 % of overburden pressure) than Experiment 1, which nearly tops at 95 % of the ice pressure (Fig. 3(b)).

Early-summer excursions of pressure in Experiment 2 ~~occur in a broad region encompassing all except the two lowermost~~ encompass all except the lowermost moulins of the Kongsfjord glaciers (Fig. 4(f)), while in Experiment ~~4~~ 1, the early-summer pressurisation of the subglacial system is ~~limited to~~ highest in the ~~upper~~ lower ablation zones of Kongsbreen and Kronebreen (Fig. 4(e))~~(Fig. 4(h))~~. Experiment 4 drives higher pressurisation of the upper ablation zones of Kongsbreen/Isachsenfonna and Kronebreen/Holtedahlfonna (Fig. 4(h)), while Experiment 3~~, despite feeding higher water volumes to the subglacial system,~~ creates lower pressures almost everywhere ~~compared to Experiment 1~~ (Fig. 4(g)) despite feeding higher water volumes to the subglacial system than Experiment 1. In July, all three Experiments 2–4 drive higher water pressures in the ablation zone and lower water pressures in the upper accumulation zone compared to Experiment 1 (Fig. 4(i–l)).

Early-summer (June) hydraulic head profiles at each terminal glacier of the Kongsfjord basin represent the height at which water would rise in boreholes drilled to the bed (Fig. 5). This figure supports model results for basal water pressure (Fig. 3(b) and Fig. 4)~~This figure supports Fig. 3(b) and Fig. 4~~, and shows that, at all glaciers except Kongsbreen North, pressure differences between the experiments are minimal at the fronts but increase slightly in the upglacier direction, with Experiments 2 and 4 generally being the highest and Experiment 3 always the lowest. At Kronebreen, water pressure typically draws near overburden pressure upstream of bedrock bumps (Fig. 5(c, d)).

~~In July, pressure biases between the experiments decrease but keep a similar pattern as in June, except that for Experiment 4 the pressure excursions cluster around regions of higher moulin density (Fig. 4(l)). The mid-summer maximum in basal water pressure (~55–65 % of the ice overburden pressure) is quasi-simultaneous with the peak in water input (end of July) in all scenarios, except in Experiment 2, which produces a significantly earlier peak in basal pressure (Fig. 3(b)). During the second half of the melt season, Experiment 1 consistently drives higher pressures, whereas Experiments 2–4 have closer agreement (Fig. 3(b)).~~

Over the mean annual period, largest discrepancies are found between Experiment 1 and Experiment 3, showing highest (~~17.4~~ 65.0 %) and lowest (~~13.3~~ 59.4 %) mean annual water pressures, respectively (Fig. 3(b)). A recurrent pattern ~~in all experiments~~ at any season is that Experiments 2–4 have systematically lower mean water pressures than Experiment 1 in the upper accumulation zones (Fig. 4). This is because in these configurations, meltwater from the upper reaches is supraglacially routed downstream before entering the subglacial system at moulins.

4.1.3 Subglacial discharge

We first investigate the partitioning of the subglacial drainage between the distributed sheet and the channels (Fig. 6). ~~In all experiments, the sudden rise in water supply at the start of the melt season rapidly increases the discharge in the distributed sheet without immediately activating channel development. In the upper model domain, the subglacial system remains inefficient throughout the summer, with almost no channel discharge (Fig. 6(a, d)). The sheet responses are relatively similar in all scenarios, except for Experiment 2, which drives an earlier rise but a lower peak in sheet discharge. In the lower model domain, after the initial build-up of the distributed sheet, channels take over and dominate the subglacial drainage from early~~

335 ~~July to late August (Fig. 6(e, f)). The timing of the switch from inefficient to efficient drainage differs between the water input configurations. With the highest total volume of water input and the fastest response in sheet discharge, Experiment 4 leads, followed by Experiments 2 1 3.~~ In all experiments, summertime subglacial drainage is dominated by the efficient system. In the accumulation zone, discharge is initially focused in the distributed sheet before channels take over in late July (Fig. 6(a, d)). In these upper reaches, the time of switching from inefficient to efficient drainage differs significantly between

340 the water input configurations. With the largest water supply at high-elevation moulins and the fastest response in subglacial discharge (Fig. 3(b)), Experiment 2 leads, followed by Experiments 4–3–1. In the ablation zone (Fig. 6(b, c)), channels develop more rapidly than in the upper regions, so that water drains primarily through the efficient system for most of the melt season (Fig. 6(e, f)). The hydrological switch in the subglacial drainage regime occurs earlier in Experiments 1 and 4 than in Experiments 2 and 3 (Fig. 6(e, f)), since the latter supply less or no meltwater at lower elevations (Fig. 2(b, c)). In

345 contrast to the distributed ~~system~~sheet~~, in which discharge is nearly equal for all experiments~~, discharge in the channel system varies considerably depending on the water input scenario, with the highest values driven by Experiments 2 and 4 at both Holtedahlfonna and Kronebreen (Fig. 6(a, c)), whereas at Kongsbreen, Experiments 4 and 1 yield highest channel discharge (Fig. 6(b)). Moreover, short-lived pulses in channel discharge are not always concurrent in all experiments; however, we focus our analysis away from these features because they likely originate from numerical artefacts. Indeed, as

350 GlaDS is built under the assumption of water-saturated channels, local numerical instabilities leading to short channel segments growing disproportionally large can cause unrealistically high local discharge. ~~All scenarios agree on that sheet discharge and channel discharge are lower and higher, respectively, at Kronebreen (Fig. 6(f)) than at Kongsbreen (Fig. 6(e)), revealing that subglacial drainage efficiency is not equal in all glaciers at Kongsfjord.~~

Next, we compare the distribution of subglacial flow paths in the model domain at the peak of channelization for each

355 water supply scenario. As shown in Figure 7, the water input configuration has little influence on the ~~morphology~~ main structure of the channelized system. By the end of August, all experiments produce an arborescent channel network in the lower ~~15 20~~ 30–35 km of the glaciers. Subglacial water is released into the fjord by three major channel trunks that connect the glacier fronts to the upper ablation areas of Kongsbreen North, Kronebreen and Kongsvegen. The Kronebreen main channel merges with the Kongsvegen channel at the confluence of the two glaciers and share the same subglacial outlet on

360 the southern side of their common front. While subglacial discharge flows in the general downglacier direction, channels do not align with the glacier centerlines, but instead follow the deeper parts of the bed. The complex basal topography of Kongsfjord causes ample meandering in the subglacial flow paths, regardless of the water input configuration. For instance, as highlighted in Fig. 7(a), a nunatak and a bedrock spur split the main channels of Kongsbreen North and Kronebreen, respectively. ~~At Kronebreen, a bedrock spur at about 10 km from the calving front splits the main channel into two branches,~~

365 ~~as highlighted in Fig. 7(d).~~ Regions of shallow ice and adverse slopes in the glacier beds impede channel formation and thus discontinuities occur, in particular in ~~moulin-free~~ Experiment 2 ~~1~~ (Fig. 7(~~a~~b)).

In the ablation zone, channels are better developed (higher connectivity and discharge) in Experiments 1 and 4 because these configurations both assume direct surface-to-bed meltwater transfer in the lower part of the domain (Fig. 7(a, d)). In

both scenarios, subglacial runoff at Kronebreen exits primarily through the south-side frontal outlet, while discharge at the
370 north-side frontal outlet is sustained only by a short, solitary channel (Fig. 7(a, d)). This is in disagreement with observations that suggest the north-side outlet has bigger plumes and thus higher subglacial discharge (How et al., 2017; Everett et al., (2018)). However, results of a hydrological analysis by Pramanik et al. (2020) show that Kronebreen drains through the southern outlet when subglacial water is at atmospheric pressure (open channels) and flow pathways are determined by bed topography alone. The absence of meltwater recharge in the lower domain of Experiment 3 leads to reduced and later
375 channel development in the ablation zone (Fig. 6(b, c, e, f)), thus limiting the subglacial pathways at Kronebreen to the main south-side channel and frontal outlet (Fig. 7(c)). While in Experiments 1–3–4 the efficient system is at its seasonal peak in late August, in Experiment 2 the earlier response in the subglacial hydrology implies that the channel network is already collapsing in the regions that receive less water input. Therefore, Experiment 2 yields shorter channels and lower discharge in the upper ablation zone of Kronebreen, as well as no channels in the lower part of Kongsbreen (Fig. 7(b)).

380 ~~The addition of moulins in Experiments 2–4 induces only little change in the main flow paths structure compared to Experiment 1.~~ In the accumulation zone, ~~However,~~ discrete water recharge at moulins focuses subglacial discharge in channels initiated directly downstream of moulins, thereby limiting the inland extension of channels to moulin locations. This is particularly visible at Kongsvegen, where the subglacial channel extends significantly further upstream in Experiment 1 (Fig. 7(a)) compared to Experiments 2–4, which split the channel between two moulins (Fig. 7(b–d)). In contrast to the
385 moulin experiments, sheet-only Experiment 1 produces a large number of minor channels (0.2–1.0 m^3 s^{-1}) in the upper model domain (Fig. 7(a)), which points to the predominance of a distributed drainage system, rather than a true channelized system. These channels seem topographically induced, as they lie across steep bedrock slopes and terminate in the subglacial valleys below Isachsenfonna and Holtedahlfonna. ~~produces larger and more continuous channels that reach slightly further inland. The ability of moulins to drive significant channels is nevertheless limited by the amount of surface meltwater~~
390 ~~captured in their upstream watersheds. In Experiment 4, 11 out of 19 moulins generate channels of flux larger than 1 m³·s⁻¹, but only seven of these channels reach a sufficient length to connect to a nearby preferential flow path (Fig. 7(d)).~~

~~One noticeable difference between the water input scenarios is that subglacial runoff in the Kronebreen/Holtedahlfonna system exits the glacier at different outlets. While in Experiments 1 and 2, subglacial discharge at Kronebreen exits primarily through the north-side frontal outlet (Fig. 7(a, b)), Experiments 3 and 4 drive the southern terminal branch of the Kronebreen~~
395 ~~channel to merge with the Kongsvegen channel, leading Kronebreen and Kongsvegen to share the same subglacial outlet on the southern side of their common front. In Experiment 3, most of the subglacial runoff exits through the south-side outlet (Fig. 7(c)), whereas in Experiment 4, the north-side outlet remains connected to the main channel of the Kronebreen/Holtedahlfonna system (Fig. 7(d)).~~

4.2 Seasonal evolution of the subglacial drainage system

400   Here we use the results of Experiment 4, the most realistic water supply configuration, to describe the subglacial hydrology of Kongsfjord. At the beginning of each melt season (early June), the subglacial hydrological system starts to evolve~~s~~ from its channel-free winter configuration. As rising amounts of surface-generated meltwater penetrate to the glacier beds, the inefficient subglacial drainage system rapidly becomes highly pressurised. Pressure first increases in the ablation zone, where surface melting is highest and crevasses allow immediate transfer of meltwater to the bed (Fig. 8(a)). Water flow at

405   the ice/bed interface dissipates energy through the melting of ice, thereby opening small channels where melt-opening exceeds creep closure. The first channels (0.2–1.0 m^3 s^{-1}) appear in late June, at the front of Kongsbreen North and Kronebreen ~~-~~Kongsvegen, before rapidly extending to the upper ablation zone. ~~where water pressure is the highest. Once initiated, channelization rapidly spreads upglacier in the ablation zone, with small channels opening on almost all of the mesh edges.~~

410   By mid-July, channels ~~of more significant size~~ have grown to accommodate larger water fluxes (> ~~1~~5.0 m^3 s^{-1}). In the lower half of the model domain, moulins have generated channels that connect to the main channel trunks, thereby forming an arborescent network (Fig. 8(b)). ~~have captured the discharge of the smaller conduits (Fig. 8(b)). This arborescent channel network first establishes in the lowermost part of the domain, before extending towards the upper catchment basins.~~ At the peak of the melt season (July–August), subglacial water pressure varies considerably (0–100 % of the ice overburden

415   pressure) across the Kongsfjord basin, with a domain-wide mean peak value of ~~59.2~~ 81.5 % of the ice overburden pressure. There is a strong inverse correlation between basal water pressure and bedrock topography, the most pressurised regions being the low-lying valleys below the accumulation basins and the subglacial overdeepenings in the ablation area.

  By late August, large channels (> 5.0 m^3 s^{-1}) have formed as far as ~~10–15~~ 30–35 km from the glacier fronts (Fig. 8(c)). There are no channels upstream of the highest moulins, which indicates that, in the absence of moulins, the efficient drainage

420   system would extend no further than the lower part of the accumulation zone. Although the broad-scale structure of the channelized system remains stable throughout the melt season, channels constantly rearrange to accommodate the short-lived variations in meltwater supply. ~~Many small channels also open in the upper reaches of the domain, mostly at the junction between Isachsenfonna and Holtedahlfonna. These minor channels seem topographically induced, as they lie across steep bedrock slopes and terminate in the subglacial valley just upstream of the confluence between Kronebreen and Infantfonna.~~

425   Most noticeably, ~~Despite channelization,~~ the subglacial system remains highly pressurised despite channelization, even during the second half of the melting period. In ~~some regions~~ most of the upper part of the glacier basin, basal water pressures in August (Fig. 8(c)) are up to ~~50~~ 20 % higher than in June (Fig. 8(a)) for comparable water inputs.

  Finally, towards the end of the melt season, the decrease in water supply leads to rapid closure of the subglacial channels, and the residual water ~~is drained~~drains through the distributed system. Channels in the upper reaches are the first to recede,

430   whereas at the glacier termini channels persist until ~~late September~~ early October.

5 Discussion

5.1 Model sensitivity to water supply distribution

In this study, we made various assumptions about how meltwater is delivered to the glacier beds. Here we discuss each of these approximations and how they impact the development of the subglacial drainage system in Kongsfjord.

Our reference experiment (Experiment 1) assumes direct and immediate surface-to-bed water transfer over the entire model domain, by considering each node of the mesh as a sink for the local meltwater. Despite still being commonly used in most models of subglacial hydrology (e.g. Cook et al., 2020), the assumption of perfect vertical permeability may only be appropriate in heavily crevassed glacier zones, such as the terminal part of Kronebreen. This approximation overestimates the amount of water supply to large parts of the glacier bed, in particular at higher highest elevations, but underestimates input in areas where recharge is concentrated at moulins. Accordingly, Experiment 1 drives higher water pressures and less channelization in the upper accumulation zone (Fig. 4), and hence highest mean annual pressures overall compared to the other scenarios (Fig. 3(b)).

In Experiment 2, the domain-wide total recharge is evenly distributed among 13 moulins instead of being directly fed to the subglacial hydrological system. The assumption of equal recharge at moulins is unrealistic as it implies that meltwater produced at lower elevations is injected into moulins at higher elevations. Results from this experiment can be easily compared with those of Experiment 1, since both scenarios apply the same water volume to the subglacial system (Fig. 3(a)). Experiment 2 drives highest water pressures at the onset of the melt season (Fig. 3(b)) as well as earliest and largest channel discharge in the accumulation zone (Fig. 6(a, d)), but lowest pressures in mid- and late summer (Fig. 3(b)). Experiment 2 drives an earlier but lower peak in subglacial water pressure than Experiment 1 (Fig. 3(b)), indicating This indicates that more localised local recharge favours earlier channel formation faster channelization in areas where moulins receive large volumes of water (Fig. 4(f)), and that more efficient drainage at higher regions of the glacier in early summer leads to lower pressurisation of the subglacial system during the rest of the melt season. through locally higher subglacial discharge (Fig. 6(a–c)).

In Experiment 3, the input to each moulin is collected from their upstream catchments (some of them extending beyond the model domain), generating a slightly larger total volume of water supply than in Experiments 1–2 (Fig. 3(a)). Yet paradoxically, Experiment 3 produces overall lower water pressures than Experiment 1 (Fig. 3(b), Fig. 4(g, k)) and poorer channelization in the ablation zone (Fig. 6(b, c, e, f)) compared to the other scenarios. We attribute this counterintuitive result to the water supply configuration that does not account for recharge in the ablation zone, where meltwater production is highest.

Experiment 4 aims at the most realistic representation of the actual supraglacial surface hydrology of the Kongsfjord basin by considering supraglacial streams, supraglacial lakes, moulins and crevasses. The total water volume delivered to the bed is higher than in the other experiments (Fig. 3(a)) due to the different drainage catchment definition (Fig. 23(da)).

Similar to Experiment 12, this scenario leads to both earlier and higher subglacial discharge in the ablation zone compared to Experiments 21 and 3 (Fig. 6(b, c, e, f))(Fig. 6(a–c)), thus ~~driving higher channelization~~ opening larger channels in the lower half of the model domain (Fig. 7(d))~~ablation zone (Fig. 6(b, c))~~. However, unlike Experiment 1, Experiment 4 produces a more efficient drainage in the upper half of the glacier basin as well, and therefore yields lower water pressures both in summer and in winter despite feeding larger volumes of meltwater to the subglacial system than the reference scenario. This is in line with findings by Koziol and Arnold (2018), which suggested that a more efficient drainage system in summer leads to lower water pressures in winter. This result also shows how a more upward-extended channelized drainage system, maintained by higher recharge at higher elevations, can lower glacier-wide basal pressure.

Notwithstanding these differences between the water input configurations, water pressure remains high (roughly around 70 %) during the entire melt season in all experiments (although less in Experiment 2), suggesting that channels are not very efficient at depressurising the subglacial hydrological system. As depicted in Figure 9, the subglacial water pressure displays annual hysteresis under variations in water input. Experiments 1–3–4 exhibit counter-clockwise hysteresis (Fig. 9(a, c, d)), meaning that for comparable water inputs, water pressure is significantly higher during falling recharge at the end of the melt season than during rising recharge at the start of the melt season. This indicates that water pressure continuously builds up during the melt season and only slowly decreases afterwards. This supports our interpretation that, in Experiments 1–3–4, channels contribute only very little to the modulation of subglacial water pressure in our study area. For Experiment 2, however, the relationship between water input and water pressure is more complex (Fig. 9(b)). For higher water inputs (above 60 m^3 s^{-1}), the hysteresis loop turns clockwise, indicating that the subglacial drainage system becomes more efficient with increasing recharge. This change of direction in hysteresis between mid-June and early September indicates that subglacial channels are able to exert some control, although limited, on basal water pressure, which explains why Experiment 2 yields lowest pressures in mid- and late summer (Fig. 3(b)).

~~Overall, varying the water input configuration does not drastically influence the seasonal evolution of the subglacial drainage system. All experiments lead to similar channel networks by the end of the summer (Fig. 7), albeit differences are noticeable in the transition period from an inefficient winter state towards the more efficient summer state (Fig. 6). More specifically, Experiments 2 and 4 introduce differences on how the subglacial drainage system copes with early-summer increase in water supply, leading to significantly higher water pressures at the onset of the melt season (Fig. 4(f, h)) and faster channelization in the ablation zone (Fig. 6(b, c, e, f)), which subsequently causes lower pressures in the ablation zone than in Experiment 1 (Fig. 4(j, l)).~~

5.2 Low efficiency of the subglacial drainage system

In contrast to some previous studies (e.g. Schoof, 2010; Chandler et al., 2013), we find no support that channels are able to substantially increase the efficiency of the subglacial drainage system, as water pressures remain high during the entire melting period in all of our experiments (Fig. 3(b)). ~~As depicted in Figure 9, the subglacial water pressure displays annual~~

495 ~~hysteresis under variations in water input. Experiments 1, 3, 4 exhibit strong counter-clockwise hysteresis (Fig. 9(a, c, d)), meaning that for comparable water inputs, water pressure is significantly higher during falling recharge at the end of the melt season than during rising recharge at the start of the melt season. This indicates that water pressure continuously builds up during the melt season and only slowly decreases afterwards. As also shown in Figure 3(b), the lag between water pressure changes in response to water input changes implies that, by the end of the melt season (late September), the subglacial~~

500 ~~hydrological system has not returned to its previous wintertime configuration. This supports our interpretation that channels contribute only very little to the modulation of subglacial water pressure in our study area. For Experiment 2, the relationship between water input and water pressure is more complex. At higher water inputs (above 60 m³·s⁻¹), the hysteresis loop turns clockwise (Fig. 9(b)), indicating that the subglacial drainage system becomes more efficient with increasing recharge. This change of direction in hysteresis between late June and mid August indicates that subglacial channels are able to exert some~~

505 ~~control, although limited, on basal water pressure.~~ Moreover, in our most realistic water supply scenario (Experiment 4), high water pressures (> ~~50~~90 % of the ice overburden pressure) until late summer over large parts of the model domain (Fig. 8(c)) suggest that channelization ~~only~~ occurs only at high pressurisation of the subglacial drainage system. ~~Channels of significant size (> 1 m³·s⁻¹) open but are restricted to the lower part of the model domain, and the presence of small channels in many regions of the glacier bed (Fig. 8(b, c)) also points to the predominance of a distributed drainage system, rather than~~

510 ~~a true channelized system.~~ We identify two factors behind the low efficiency of the channels in our study area.

First, ~~our model results show that the spatial distribution of channels is primarily controlled by the bed topography, regardless of the water input configuration. Channels form along steep basal slopes and basal overdeepenings, where gradients of hydraulic potential are highest. All of our experiments produce similar spatial patterns in the summertime drainage efficiency, with the largest subglacial channel occurring underneath the Kronebreen/Holtedahlfonna system. The~~

515 ~~location of the modelled channel network and its outlets in the lower part of Kronebreen is consistent with findings of How et al. (2017), who used a simpler approach for determining subglacial flow paths, assuming a static hydraulic potential. The~~ the small surface gradients that characterise our model domain ~~also~~ drive ~~the~~ high pressurisation of the channels. Subglacial channels open through melting of the overlying ice driven by turbulent heat dissipation, which requires steep~~er~~ downglacier bed and surface slopes ~~that are absent~~ than those in our study area. Hence, higher water pressures are required to counteract

520 creep closure and maintain the channels open, even in areas that receive high water input from moulins. The finding that subglacial channels do not play an important role in regulating subglacial water pressure at such low sloping glaciers has been reported in other studies applied to the Greenland Ice Sheet (Meierbachtol et al., 2013; Moon et al., 2014; Dow et al., 2015).

Second, ~~A~~arctic glaciers such as those of the Kongsfjord basin experience shorter melt seasons than mid- and low-

525 latitude glaciers, and thus receive overall less water supply from the surface, which also ~~disadvantages~~ inhibits channelization. In particular, minimal wintertime water input due to generally low temperatures in the Arctic and limited recharge from episodic warm spells is unable to sustain year-round subglacial channels. Compared to overwintered channels that more readily grow to accommodate meltwater input, first season channels lack the capacity to evacuate large volumes of

water injected to glacier beds. Poinar et al. (2019) suggested that high-evelation firn aquifers can provide steady water input to the subglacial system outside of the melt season, thereby facilitating subglacial channel formation and winter-persistence, even in low sloping areas. Evidence of a perennial firn aquifer was revealed by ice-penetrating radar and GPS observations in the upper reaches of Holtedahlfonna (Christianson et al., 2015). This aquifer is recharged by downward percolation of summertime meltwater, and discharge occurs through downhill flow in the winter. Deep firn water storage is accounted for in the model that provided the input time series to our subglacial hydrology model (Van Pelt et al., 2019), but does not permit considerable wintertime contribution to recharge in the absence of supply from the surface.

5.3 Implications for glacier sliding

Studies of glacier motion suggest that ice acceleration typically occurs after the onset of the melt season, when water input to the ice/bed interface is rising faster than the subglacial drainage system can accommodate, driving an increase in basal water pressure, ice-bed separation, and sliding. The sensitivity of ice motion to water input usually decreases over the melt season as the subglacial drainage system evolves from an inefficient distributed to efficient channelized configuration, thereby gradually lowering basal water pressures despite increasing surface melt, and thus causing ice deceleration in late summer (Davison et al., 2019).

Instead, our model results show that basal water pressures remain high during the entire summer, which we attribute to low hydraulic gradients that in turn disfavour the development of efficient channels. We found that varying the water input configuration introduces differences in the way the subglacial drainage system copes with the early-summer increase in water supply, which may be crucial for glacier sliding. In an ice flow model forced by a subglacial hydrology model such as that used in this study, Experiment 1 would cause unrealistically high sliding in the upper accumulation zone as these regions receive too much water. Conversely, the absence of water recharge in the ablation zone (Experiment 3), in driving only moderate pressurisation of the subglacial system, would underestimate the rate of sliding at lower elevations. Our results also suggest that limited efficiency of the channelized system, which we attribute to low hydraulic gradients, further enhances sensitivity of sliding to basal recharge variability by maintaining high water pressures and faster sliding speed during the entire summer. We thence deduce that substantial sliding likely occurs at most of the Kongsfjord glaciers over the entire melt season, and that sliding rates remain high even in the late summer, which is consistent with observations by Schellenberger et al. (2015) for Kronebreen. For Kongsbreen North, however, Schellenberger et al. (2015) show that surface velocities tend to decrease over the melt season, which is not in accordance with our findings. Their results suggest that subglacial drainage efficiency increases during summer and is able to lower water pressure in that part of the glacier system. Such behaviour is not captured by our model and may be due to the existence of permanent canals carved in the subglacial sediment (Walder and Fowler, 1994), which are not accounted for in the GlaDS model.

Limited channelization, by maintaining high water pressures in the subglacial system, further enhances sensitivity of sliding to basal recharge variability.

~~565~~
~~570~~

5.4 Model limitations and future work

One limitation of this study is the lack of coupling between subglacial hydrology and ice dynamics. Given the regional scale of our experiments, running the model in an uncoupled version allowed us to keep the computational cost of our study at a
575 reasonable level. Therefore, we have primarily focused our discussion on the behaviour of the subglacial hydrological system under different melt input configurations, and have only cautiously discussed its likely impacts on sliding. Implementing a two-way coupled model would be relevant for future studies seeking to investigate in more detail the feedbacks between subglacial hydrology and ice dynamics.

Another limitation is that our modelling approach ignores some aspects of the glacial hydrological system. We assume
580 that the location of surface-to-bed connections such as moulins and crevasses remains unchanged during the ~~15-year~~ 14-year period of our simulations. In reality, supraglacial hydrology is a dynamic system that is governed by variations in ice velocity and in surface mass balance. Glacier acceleration enhances crevassing, thus increasing the area of direct meltwater transfer to the ice/bed interface. Intense melt events not only promote opening of new moulins through melt-enlargement of existing crevasses, but also drive hydrofracturing, a mechanism through which water-filled crevasses or supraglacial
585 meltwater ponds abruptly propagate downwards (Alley et al., 2005, van der Veen, 2007; Das et al., 2008). Supraglacial lake drainage is a widespread mechanism for moulin activation in the upper ablation zone, and hence may contribute significantly to subglacial reorganisation (Bingham et al., 2003; Andrews et al., 2018; Hoffman et al., 2018). Firn aquifers lying upstream of crevasse fields can also drive hydrofracturing (Poinar et al., 2017). Consequently, neglecting the spatiotemporal evolution of crevasses, moulins and lake drainage events in our model is definitely a limiting factor to the accurate simulation of water
590 recharge to glacier beds. This limitation could be overcome by using a spatially distributed model of supraglacial hydrology that would predict both the location and the timing of new surface-to-bed hydrological connections for given surface melt scenarios (e.g. Clason et al., 2012; 2015; Koziol et al., 2017).

Finally, the GlaDS model is built on hard-bed physics that may not be relevant everywhere in our study area. The presence of abundant sediment alters water drainage at the glacier base, as water can also flow through porous sediment or canals carved in the sediment (Walder and Fowler, 1994), for instance. While GlaDS includes the presence of porous sediment through the parameter of water sheet conductivity, the model does not account for formation of canals within the sediment. Canals could locally increase drainage efficiency compared to the prediction obtained from the Röthlisberger (1972) theory alone as implemented in GlaDS.

6 Conclusions

The results of our modelling indicate that discrete basal water recharge at moulins (Experiments 2 and 4) leads to higher water pressures at the beginning of the melt season, exceeding those simulated when assuming spatially continuous, direct surface-to-bed transfer (Experiment 1). However, the more localised recharge also favours a faster evolution of subglacial channels, with an opposite effect that quickly dominates such that the moulin configurations (Experiments 2–3–4) result in overall lower water pressures during the remaining of the melt season and the subsequent winter. The modelled timing at which sliding would start to occuraccelerate is therefore sensitive to moulin distribution and total basal recharge. In this regard, we conclude that there is value in mapping of supraglacial hydrology features such as streams, crevasses, lakes and moulins in order to appropriately represent recharge to the subglacial drainage system.improve constraining of recharge to glacier beds and accurately determine the distribution of meltwater input into moulins.

Nevertheless, our model resultsDespite differences in the subglacial hydrological response to early-summer rise in meltwater supply, all of our experiments agree suggest that the modelled subglacial hydrology in our study area has limited sensitivity to is overall poorly sensitive to the water input configuration. We find that both the location and the size of subglacial channels are governed largely by basal topography, regardless of how and where water enters the glacier beds, and that channels remain highly pressurised during the entire melt season. We attribute this to the gentle slopes of the glaciers that do not support strong hydraulic gradients and to the short duration of the high Aarctic melt season with limited amounts of meltwater injected to the subglacial hydrological system. Therefore, subglacial channels are unable to substantially decrease the summertime overall basal pressure, implying that sliding is directly linked to spatiotemporal variability in meltwater recharge, and that sliding likely occurs at the Kongsfjord basin during the entire melting period.

The outcomes of our study raise implications for the future of ice dynamics in a warming climate and can be generalised to most Svalbard tidewater glaciers, which have relatively flat surfaces and which experience typically less water supply to their beds due to their high latitude. The inability of these glaciers to build an efficient drainage system implies that they are likely sensitive to long-term trends in meltwater supply variability, contrary to what would be expected in a more standard configuration (Schoof, 2010).

Data availability

The digital elevation model can be accessed at https://doi.org/10.21334/npolar.2014.dce53a47 (Norwegian Polar Institute, 2014). The
625 glacier and land masks were constructed from glacier outlines, which are available at https://doi.org/10.21334/npolar.2013.89f430f8
(König et al., 2013). The subglacial topography and bathymetry of Kongsfjorden is available at
https://doi.org/10.21334/npolar.2017.702ca4a7 (Lindbäck et al. 2018). The modelled water recharge dataset has been prepared and shared
by Ward Van Pelt, and can also be accessed in the following repository: https://doi.org/10.6084/m9.figshare.7836530.v1 (Van Pelt et al.
2019). Crevasse zones and moulin locations have been mapped from commercially available, licenced satellite imagery (CNES (2014) and
630 Airbus DS (2014), all rights reserved. Commercial uses forbidden). The TopoToolbox is available at
https://github.com/wschwanghart/topotoolbox (Schwanghart and Scherler, 2014). The subglacial hydrology model GlaDS is freely
available as part of the Elmer/Ice model (Gagliardini and Werder, 2018). The underlying model outputs for the figures presented in this
paper can be accessed at https://doi.org/10.5281/zenodo.4680908.

Author contributions

635 All three authors designed the research idea, CS performed the simulations and the main analysis. CS wrote the paper with contributions
from all co-authors.

Competing interests

The authors declare that they have no conflict of interest.

Acknowledgements

640 The authors would like to thank Ward Van Pelt for providing the water recharge time series used as input to the subglacial hydrology
model. We are grateful to Jack Kohler and Chris Nuth for their support in obtaining and processing digital elevation models and satellite
imagery. Chloé Scholzen would like to thank Olivier Gagliardini for fruitful discussions and assistance during her research stay at IGE,
CNRS.

Financial support

645 This research has been supported by the Norwegian Ministry of Education and Research who granted a PhD fellowship to CS, and the
Research Council of Norway through the project MAMMAMIA (grant no. 301837).

References

(AMAP), A. M. a. A. P.: Snow, Water, Ice and Permafrost in the Arctic (SWIPA); Summary for Policy-makers, 2017.

Alley, R. B., Dupont, T. K., Parizek, B. R., and Anandakrishnan, S.: Access of surface meltwater to beds of sub-freezing glaciers:
650  preliminary insights, Annals of Glaciology, 40, 8-14, 2005.

Andrews, L. C., Hoffman, M. J., Neumann, T. A., Catania, G. A., Lüthi, M. P., Hawley, R. L., Schild, K. M., Ryser, C., and Morriss, B. F.:
  Seasonal evolution of the subglacial hydrologic system modified by supraglacial lake drainage in western Greenland, Journal of
  Geophysical Research: Earth Surface, 123, 1479-1496, 2018.

Banwell, A., Hewitt, I., Willis, I., and Arnold, N.: Moulin density controls drainage development beneath the Greenland ice sheet, Journal
655  of Geophysical Research: Earth Surface, 121, 2248-2269, 2016.

Bartholomew, I., Nienow, P., Mair, D., Hubbard, A., King, M. A., and Sole, A.: Seasonal evolution of subglacial drainage and acceleration
  in a Greenland outlet glacier, Nature Geoscience, 3, 408-411, 2010.

Benn, D. I., and Evans, D. J. A.: Glaciers and Glaciation, 2nd ed., Hodder Education, London, UK, 802 pp., 2010.

Bindschadler, R.: The importance of pressurized subglacial water in separation and sliding at the glacier bed, Journal of Glaciology, 29, 3-
660  19, 1983.

Bingham, R. G., Nienow, P. W., and Sharp, M. J.: Intra-annual and intra-seasonal flow dynamics of a High Arctic polythermal valley
  glacier, Annals of Glaciology, 37, 181-188, 2003.

Björnsson, H., Gjessing, Y., Hamran, S.-E., Hagen, J. O., Liestøl, O., Pálsson, F., and Erlingsson, B.: The thermal regime of sub-polar
  glaciers mapped by multi-frequency radio-echo sounding, Journal of Glaciology, 42, 23-32, 1996.

665 Bouillon, A., Bernard, M., Gigord, P., Orsoni, A., Rudowski, V., and Baudoin, A.: SPOT 5 HRS geometric performances: Using block
  adjustment as a key issue to improve quality of DEM generation, ISPRS Journal of Photogrammetry and Remote Sensing, 60, 134-
  146, 2006.

Bueler, E., and Van Pelt, W.: Mass-conserving subglacial hydrology in the Parallel Ice Sheet Model version 0.6, Geoscientific Model
  Development, 2015.

670 Carey, M., Molden, O. C., Rasmussen, M. B., Jackson, M., Nolin, A. W., and Mark, B. G.: Impacts of glacier recession and declining
  meltwater on mountain societies, Annals of the American Association of Geographers, 107, 350-359, 2017.

Catania, G. A., and Neumann, T.: Persistent englacial drainage features in the Greenland Ice Sheet, Geophysical Research Letters, 37,
  2010.

Chandler, D., Wadham, J., Lis, G., Cowton, T., Sole, A., Bartholomew, I., Telling, J., Nienow, P., Bagshaw, E., and Mair, D.: Evolution of
675  the subglacial drainage system beneath the Greenland Ice Sheet revealed by tracers, Nature Geoscience, 6, 195-198, 2013.

Christianson, K., Kohler, J., Alley, R. B., Nuth, C., and Van Pelt, W. J.: Dynamic perennial firn aquifer on an Arctic glacier, Geophysical
  Research Letters, 42, 1418-1426, 2015.

Clason, C., Mair, D., Burgess, D., and Nienow, P.: Modelling the delivery of supraglacial meltwater to the ice/bed interface: application to
  southwest Devon Ice Cap, Nunavut, Canada, Journal of Glaciology, 58, 361-374, 2012.

680 Clason, C., Mair, D., Nienow, P., Bartholomew, I., Sole, A., Palmer, S., and Schwanghart, W.: Modelling the transfer of supraglacial
  meltwater to the bed of Leverett Glacier, Southwest Greenland, Earth's Cryosphere, 2015.

Cook, S. J., Christoffersen, P., Todd, J., Slater, D., and Chauché, N.: Coupled modelling of subglacial hydrology and calving-front melting
  at Store Glacier, West Greenland, The Cryosphere, 2020.

Copland, L., Sharp, M. J., and Nienow, P. W.: Links between short-term velocity variations and the subglacial hydrology of a
685  predominantly cold polythermal glacier, Journal of Glaciology, 49, 337-348, 2003.

Cowton, T., Nienow, P., Sole, A., Wadham, J., Lis, G., Bartholomew, I., Mair, D., and Chandler, D.: Evolution of drainage system morphology at a land-terminating Greenlandic outlet glacier, Journal of Geophysical Research: Earth Surface, 118, 29-41, 2013.

Das, S. B., Joughin, I., Behn, M. D., Howat, I. M., King, M. A., Lizarralde, D., and Bhatia, M. P.: Fracture propagation to the base of the Greenland Ice Sheet during supraglacial lake drainage, Science, 320, 778-781, 2008.

690   Davison, B. J., Sole, A. J., Livingstone, S. J., Cowton, T. R., and Nienow, P. W.: The influence of hydrology on the dynamics of land-terminating sectors of the Greenland Ice Sheet, Frontiers in Earth Science, 7, 2019.

de Fleurian, B., Gagliardini, O., Zwinger, T., Durand, G., Le Meur, E., Mair, D., and Raback, P.: A double continuum hydrological model for glacier applications, The Cryosphere, 2014.

de Fleurian, B., Werder, M. A., Beyer, S., Brinkerhoff, D. J., Delaney, I., Dow, C. F., Downs, J., Gagliardini, O., Hoffman, M. J., and
695   Hooke, R. L.: SHMIP The subglacial hydrology model intercomparison Project, Journal of Glaciology, 64, 897-916, 2018.

Decaux, L., Grabiec, M., Ignatiuk, D., and Jania, J.: Role of discrete water recharge from supraglacial drainage systems in modeling patterns of subglacial conduits in Svalbard glaciers, The Cryosphere, 13, 735-752, 2019.

Dow, C. F., Kulessa, B., Rutt, I., Tsai, V., Pimentel, S., Doyle, S., Van As, D., Lindbäck, K., Pettersson, R., and Jones, G.: Modeling of subglacial hydrological development following rapid supraglacial lake drainage, Journal of Geophysical Research: Earth Surface, 120,
700   1127-1147, 2015.

Dow, C. F., Werder, M., Babonis, G., Nowicki, S., Walker, R. T., Csathó, B., and Morlighem, M.: Dynamics of active subglacial lakes in Recovery Ice Stream, Journal of Geophysical Research: Earth Surface, 123, 837-850, 2018.

Dow, C. F., McCormack, F., Young, D., Greenbaum, J., Roberts, J., and Blankenship, D.: Totten Glacier subglacial hydrology determined from geophysics and modeling, Earth and Planetary Science Letters, 531, 115961, 2020.

705   Downs, J. Z., Johnson, J. V., Harper, J. T., Meierbachtol, T., and Werder, M. A.: Dynamic hydraulic conductivity reconciles mismatch between modeled and observed winter subglacial water pressure, Journal of Geophysical Research: Earth Surface, 123, 818-836, 2018.

Dunse, T., Schuler, T., Hagen, J., and Reijmer, C.: Seasonal speed-up of two outlet glaciers of Austfonna, Svalbard, inferred from continuous GPS measurements, The Cryosphere, 6, 453-466, 2012.

Dunse, T., Schellenberger, T., Hagen, J. O. M., Kääb, A., Schuler, T. V., and Reijmer, C.: Glacier-surge mechanisms promoted by a
710   hydro-thermodynamic feedback to summer melt, The Cryosphere, 9, 197-215, 2015.

Everett, A., Kohler, J., Sundfjord, A., Kovacs, K. M., Torsvik, T., Pramanik, A., Boehme, L., and Lydersen, C.: Subglacial discharge plume behaviour revealed by CTD-instrumented ringed seals, Scientific reports, 8, 1-10, 2018.

Flowers, G. E., and Clarke, G. K.: A multicomponent coupled model of glacier hydrology 1. Theory and synthetic examples, Journal of Geophysical Research: Solid Earth, 107, ECV 9-1-ECV 9-17, 2002.

715   Flowers, G. E.: Modelling water flow under glaciers and ice sheets, Proceedings of the Royal Society A: Mathematical, Physical and Engineering Sciences, 471, 20140907, 2015.

Fountain, A. G., Campbell, J. L., Schuur, E. A., Stammerjohn, S. E., Williams, M. W., and Ducklow, H. W.: The disappearing cryosphere: impacts and ecosystem responses to rapid cryosphere loss, BioScience, 62, 405-415, 2012.

Gagliardini, O., Zwinger, T., Gillet-Chaulet, F., Durand, G., Favier, L., De Fleurian, B., Greve, R., Malinen, M., Martín, C., and Råback,
720   P.: Capabilities and performance of Elmer/Ice, a new-generation ice sheet model, Geoscientific Model Development, 6, 1299-1318, 2013.

Gagliardini, O., and Werder, M. A.: Influence of increasing surface melt over decadal timescales on land-terminating Greenland-type outlet glaciers, Journal of Glaciology, 64, 700-710, 2018.

Gulley, J., Benn, D., Müller, D., and Luckman, A.: A cut-and-closure origin for englacial conduits in uncrevassed regions of polythermal glaciers, Journal of Glaciology, 55, 66-80, 2009a.

Gulley, J., Benn, D., Screaton, E., and Martin, J.: Mechanisms of englacial conduit formation and their implications for subglacial recharge, Quaternary Science Reviews, 28, 1984-1999, 2009b.

Gulley, J., Grabiec, M., Martin, J., Jania, J., Catania, G., and Glowacki, P.: The effect of discrete recharge by moulins and heterogeneity in flow-path efficiency at glacier beds on subglacial hydrology, Journal of Glaciology, 58, 926-940, 2012.

Hagen, J., Melvold, K., Eiken, T., Isaksson, E., and Lefauconnier, B.: Mass balance methods on Kongsvegen, Svalbard, Geografiska Annaler: Series A, Physical Geography, 81, 593-601, 1999.

Hagen, J. O., Eiken, T., Kohler, J., and Melvold, K.: Geometry changes on Svalbard glaciers: mass-balance or dynamic response?, Annals of Glaciology, 42, 255-261, 2005.

Hewitt, I. J.: Modelling distributed and channelized subglacial drainage: the spacing of channels, Journal of Glaciology, 57, 302-314, 2011.

Hewitt, I. J.: Seasonal changes in ice sheet motion due to melt water lubrication, Earth and Planetary Science Letters, 371, 16-25, 2013.

Hoffman, M., and Price, S.: Feedbacks between coupled subglacial hydrology and glacier dynamics, Journal of Geophysical Research: Earth Surface, 119, 414-436, 2014.

Hoffman, M., Perego, M., Andrews, L. C., Price, S. F., Neumann, T. A., Johnson, J. V., Catania, G., and Lüthi, M. P.: Widespread moulin formation during supraglacial lake drainages in Greenland, Geophysical Research Letters, 45, 778-788, 2018.

Horgan, H. J., Anderson, B., Alley, R. B., Chamberlain, C. J., Dykes, R., Kehrl, L. M., and Townend, J.: Glacier velocity variability due to rain-induced sliding and cavity formation, Earth and Planetary Science Letters, 432, 273-282, 2015.

How, P., Benn, D. I., Hulton, N. R., Hubbard, B., Luckman, A., Sevestre, H., Van Pelt, W. J., Lindbäck, K., Kohler, J., and Boot, W.: Rapidly changing subglacial hydrological pathways at a tidewater glacier revealed through simultaneous observations of water pressure, supraglacial lakes, meltwater plumes and surface velocities, Cryosphere, 2691-2710, 2017.

Iken, A., Röthlisberger, H., Flotron, A., and Haeberli, W.: The uplift of Unteraargletscher at the beginning of the melt season—a consequence of water storage at the bed?, Journal of glaciology, 29, 28-47, 1983.

Iken, A., and Bindschadler, R. A.: Combined measurements of subglacial water pressure and surface velocity of Findelengletscher, Switzerland: conclusions about drainage system and sliding mechanism, Journal of Glaciology, 32, 101-119, 1986.

Iken, A., and Truffe, M.: The relationship between subglacial water pressure and velocity of Findelengletscher, Switzerland, during its advance and retreat, Journal of Glaciology, 43, 328-338, 1997.

Joughin, I., Das, S. B., Flowers, G., Behn, M. D., Alley, R. B., King, M. A., Smith, B., Bamber, J., van den Broeke, M. R., and Van Angelen, J.: Influence of ice-sheet geometry and supraglacial lakes on seasonal ice-flow variability, The Cryosphere, 7, 1185-1192, 2013.

Kääb, A., Lefauconnier, B., and Melvold, K.: Flow field of Kronebreen, Svalbard, using repeated Landsat 7 and ASTER data, Annals of Glaciology, 42, 7-13, 2005.

Kamb, B.: Glacier surge mechanism based on linked cavity configuration of the basal water conduit system, Journal of Geophysical Research: Solid Earth, 92, 9083-9100, 1987.

Kehrl, L. M., Hawley, R. L., Powell, R. D., and Brigham-Grette, J.: Glacimarine sedimentation processes at Kronebreen and Kongsvegen, Svalbard, Journal of Glaciology, 57, 841-847, 2011.

König, M., Kohler, J., and Nuth, C.: Glacier area outlines–Svalbard [Data set], Norwegian Polar Institute.(doi: 10.21334/npolar. 2013.89 f430f8), 2013.

Korona, J., Berthier, E., Bernard, M., Rémy, F., and Thouvenot, E.: SPIRIT. SPOT 5 stereoscopic survey of polar ice: reference images and topographies during the fourth International Polar Year (2007–2009), ISPRS Journal of Photogrammetry and Remote Sensing, 64, 204-212, 2009.

Koziol, C., Arnold, N., Pope, A., and Colgan, W.: Quantifying supraglacial meltwater pathways in the Paakitsoq region, West Greenland, Journal of Glaciology, 63, 464-476, 2017.

Koziol, C. P., and Arnold, N.: Modelling seasonal meltwater forcing of the velocity of land-terminating margins of the Greenland Ice Sheet, The Cryosphere, 12, 971-991, 2018.

Lefauconnier, B.: Fluctuations glaciaires dans le Kongsfjord, bai du Roi, 79 N, Spitsbergen, analyses et conseqences (Glacier fluctuations in Kongsfjorden, 79 N, Spitsbergen, analyses and consequences), Unpublished thesis. Universite de Grenoble, 1987.

Lefauconnier, B., Hagen, J. O., and Rudant, J. P.: Flow speed and calving rate of Kongsbreen glacier, Svalbard, using SPOT images, Polar Research, 13, 59-65, 1994a.

Lefauconnier, B., Hagen, J. O., Pinglot, J. F., and Pourchet, M.: Mass-balance estimates on the glacier complex Kongsvegen and Sveabreen, Spitsbergen, Svalbard, using radioactive layers, Journal of Glaciology, 40, 368-376, 1994b.

Liestøl, O.: The glaciers in the Kongsfjorden area, Spitsbergen, Norsk Geografisk Tidsskrift-Norwegian Journal of Geography, 42, 231-238, 1988.

Lindbäck, K., Kohler, J., Pettersson, R., Nuth, C., Langley, K., Messerli, A., Vallot, D., Keniche, M., and Brandt, O.: Subglacial topography, ice thickness, and bathymetry of Kongsfjorden, northwestern Svalbard, Earth System Science Data, 10, 2018a.

Lliboutry, L.: General theory of subglacial cavitation and sliding of temperate glaciers, Journal of Glaciology, 7, 21-58, 1968.

Mair, D., Nienow, P., Willis, I., and Sharp, M.: Spatial patterns of glacier motion during a high-velocity event: Haut Glacier d'Arolla, Switzerland, Journal of Glaciology, 47, 9-20, 2001.

Meierbachtol, T., Harper, J., and Humphrey, N.: Basal drainage system response to increasing surface melt on the Greenland ice sheet, Science, 341, 777-779, 2013.

Melvold, K., and Hagen, J. O.: Evolution of a surge-type glacier in its quiescent phase: Kongsvegen, Spitsbergen, 1964–95, Journal of Glaciology, 44, 394-404, 1998.

Milner, A. M., Khamis, K., Battin, T. J., Brittain, J. E., Barrand, N. E., Füreder, L., Cauvy-Frauni é, S., Gíslason, G. M., Jacobsen, D., and Hannah, D. M.: Glacier shrinkage driving global changes in downstream systems, Proceedings of the National Academy of Sciences, 114, 9770-9778, 2017.

Moon, T., Joughin, I., Smith, B., Van Den Broeke, M. R., Van De Berg, W. J., Noël, B., and Usher, M.: Distinct patterns of seasonal Greenland glacier velocity, Geophysical research letters, 41, 7209-7216, 2014.

Nienow, P., Sharp, M., and Willis, I.: Seasonal changes in the morphology of the subglacial drainage system, Haut Glacier d'Arolla, Switzerland, Earth Surface Processes and Landforms: The Journal of the British Geomorphological Group, 23, 825-843, 1998.

Nuth, C., Schuler, T. V., Kohler, J., Altena, B., and Hagen, J. O.: Estimating the long-term calving flux of Kronebreen, Svalbard, from geodetic elevation changes and mass-balance modeling, Journal of Glaciology, 58, 119-133, 2012.

Nuth, C., Gilbert, A., Köhler, A., McNabb, R., Schellenberger, T., Sevestre, H., Weidle, C., Girod, L., Luckman, A., and Kääb, A.: Dynamic vulnerability revealed in the collapse of an Arctic tidewater glacier, Scientific reports, 9, 1-13, 2019.

Pfeffer, W. T., Meier, M. F., and Illangasekare, T. H.: Retention of Greenland runoff by refreezing: implications for projected future sea level change, Journal of Geophysical Research: Oceans, 96, 22117-22124, 1991.

800   Pimentel, S., and Flowers, G. E.: A numerical study of hydrologically driven glacier dynamics and subglacial flooding, Proceedings of the Royal Society A: Mathematical, Physical and Engineering Sciences, 467, 537-558, 2011.

Poinar, K., Joughin, I., Lilien, D., Brucker, L., Kehrl, L., and Nowicki, S.: Drainage of Southeast Greenland firn aquifer water through crevasses to the bed, Frontiers in Earth Science, 5, 5, 2017.

Poinar, K., Dow, C. F., and Andrews, L. C.: Long-Term Support of an Active Subglacial Hydrologic System in Southeast Greenland by
805   Firn Aquifers, Geophysical Research Letters, 46, 4772-4781, 2019.

Pörtner, H., Roberts, D., Masson-Delmotte, V., Zhai, P., Tignor, M., Poloczanska, E., Mintenbeck, K., Nicolai, M., Okem, A., and Petzold, J.: IPCC, 2019: IPCC Special Report on the Ocean and Cryosphere in a Changing Climate, 2019.

Pramanik, A., Kohler, J., Lindbäck, K., How, P., Van Pelt, W., Liston, G., and Schuler, T. V.: Hydrology and runoff routing of glacierized drainage basins in the Kongsfjord area, northwest Svalbard, The Cryosphere Discussions, 1-33, 2020.

810   Röthlisberger, H.: Water pressure in intra-and subglacial channels, Journal of Glaciology, 11, 177-203, 1972.

Schellenberger, T., Dunse, T., Kääb, A., Kohler, J., and Reijmer, C.: Surface speed and frontal ablation of Kronebreen and Kongsbreen, NW-Svalbard, from SAR offset tracking, The Cryosphere Discussions, 8, 6193-6233, 2015.

Schild, K. M., Hawley, R. L., and Morriss, B. F.: Subglacial hydrology at Rink Isbræ, West Greenland inferred from sediment plume appearance, Annals of Glaciology, 57, 118-127, 2016.

815   Schoof, C.: Ice-sheet acceleration driven by melt supply variability, Nature, 468, 803-806, 2010.

Schwanghart, W., and Scherler, D.: TopoToolbox 2–MATLAB-based software for topographic analysis and modeling in Earth surface sciences, Earth Surface Dynamics, 2, 1-7, 2014.

Sevestre, H., Benn, D. I., Hulton, N. R., and Bælum, K.: Thermal structure of Svalbard glaciers and implications for thermal switch models of glacier surging, Journal of Geophysical Research: Earth Surface, 120, 2220-2236, 2015.

820   Slater, D., Nienow, P., Sole, A., Cowton, T., Mottram, R., Langen, P., and Mair, D.: Spatially distributed runoff at the grounding line of a large Greenlandic tidewater glacier inferred from plume modelling, Journal of Glaciology, 63, 309-323, 2017.

Sole, A. J., Mair, D. W. F., Nienow, P. W., Bartholomew, I., King, M., Burke, M. J., and Joughin, I.: Seasonal speedup of a Greenland marine-terminating outlet glacier forced by surface melt–induced changes in subglacial hydrology, Journal of Geophysical Research: Earth Surface, 116, 2011.

825   Sugiyama, S., and Gudmundsson, G. H.: Short-term variations in glacier flow controlled by subglacial water pressure at Lauteraargletscher, Bernese Alps, Switzerland, Journal of Glaciology, 50, 353-362, 2004.

Sund, M., Eiken, T., and Rolstad Denby, C.: Velocity structure, front position changes and calving of the tidewater glacier Kronebreen, Svalbard, The Cryosphere Discussions, 5, 41-73, 2011.

Sundal, A. V., Shepherd, A., Nienow, P., Hanna, E., Palmer, S., and Huybrechts, P.: Melt-induced speed-up of Greenland ice sheet offset
830   by efficient subglacial drainage, Nature, 469, 521-524, 2011.

Svendsen, H., Beszczynska-Møller, A., Hagen, J. O., Lefauconnier, B., Tverberg, V., Gerland, S., Børre Ørbæk, J., Bischof, K., Papucci, C., and Zajaczkowski, M.: The physical environment of Kongsfjorden–Krossfjorden, an Arctic fjord system in Svalbard, Polar research, 21, 133-166, 2002.

835 Trusel, L. D., Powell, R., Cumpston, R., and Brigham-Grette, J.: Modern glacimarine processes and potential future behaviour of Kronebreen and Kongsvegen polythermal tidewater glaciers, Kongsfjorden, Svalbard, Geological Society, London, Special Publications, 344, 89-102, 2010.

Vallot, D., Pettersson, R., Luckman, A., Benn, D. I., Zwinger, T., Van Pelt, W. J., Kohler, J., Schäfer, M., Claremar, B., and Hulton, N. R.: Basal dynamics of Kronebreen, a fast-flowing tidewater glacier in Svalbard: non-local spatio-temporal response to water input, Journal of Glaciology, 63, 1012-1024, 2017.

840 van der Veen, C. J.: Fracture propagation as means of rapidly transferring surface meltwater to the base of glaciers, Geophysical Research Letters, 34, 2007.

Van Pelt, W., and Kohler, J.: Modelling the long-term mass balance and firn evolution of glaciers around Kongsfjorden, Svalbard, Journal of Glaciology, 61, 731-744, 2015.

Van Pelt, W., Pohjola, V., Pettersson, R., Marchenko, S., Kohler, J., Luks, B., Hagen, J. O., Schuler, T., Dunse, T., and Noël, B.: A long-845 term dataset of climatic mass balance, snow conditions, and runoff in Svalbard (1957–2018), The Cryosphere, 13, 2259-2280, 2019.

Van Pelt, W. J., Pohjola, V. A., and Reijmer, C. H.: The changing impact of snow conditions and refreezing on the mass balance of an idealized Svalbard glacier, Frontiers in Earth Science, 4, 102, 2016.

Vincent, W. F., Callaghan, T. V., Dahl-Jensen, D., Johansson, M., Kovacs, K. M., Michel, C., Prowse, T., Reist, J. D., and Sharp, M.: Ecological implications of changes in the Arctic cryosphere, Ambio, 40, 87-99, 2011.

850 Walder, J. S., and Fowler, A.: Channelized subglacial drainage over a deformable bed, Journal of Glaciology, 40, 3-15, 1994.

Werder, M. A., and Schuler, T. V.: Short term variations of tracer transit speed on alpine glaciers, The Cryosphere, 4, 381-396, 2010.

Werder, M. A., Hewitt, I. J., Schoof, C. G., and Flowers, G. E.: Modeling channelized and distributed subglacial drainage in two dimensions, Journal of Geophysical Research: Earth Surface, 118, 2140-2158, 2013.

Wouters, B., Gardner, A. S., and Moholdt, G.: Global glacier mass loss during the GRACE satellite mission (2002-2016), Frontiers in 855 earth science, 7, 96, 2019.

Wyatt, F. R., and Sharp, M. J.: Linking surface hydrology to flow regimes and patterns of velocity variability on Devon Ice Cap, Nunavut, Journal of Glaciology, 61, 387-399, 2015.

Zwally, H. J., Abdalati, W., Herring, T., Larson, K., Saba, J., and Steffen, K.: Surface melt-induced acceleration of Greenland ice-sheet flow, Science, 297, 218-222, 2002.

860
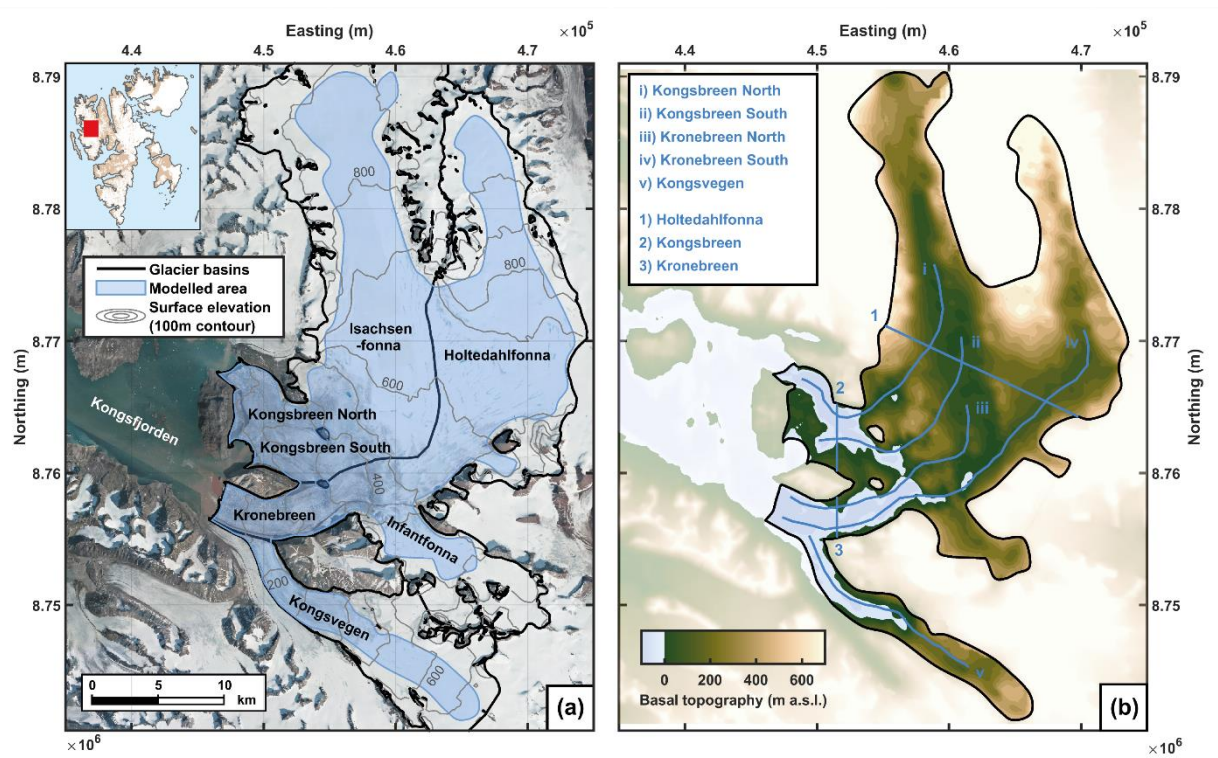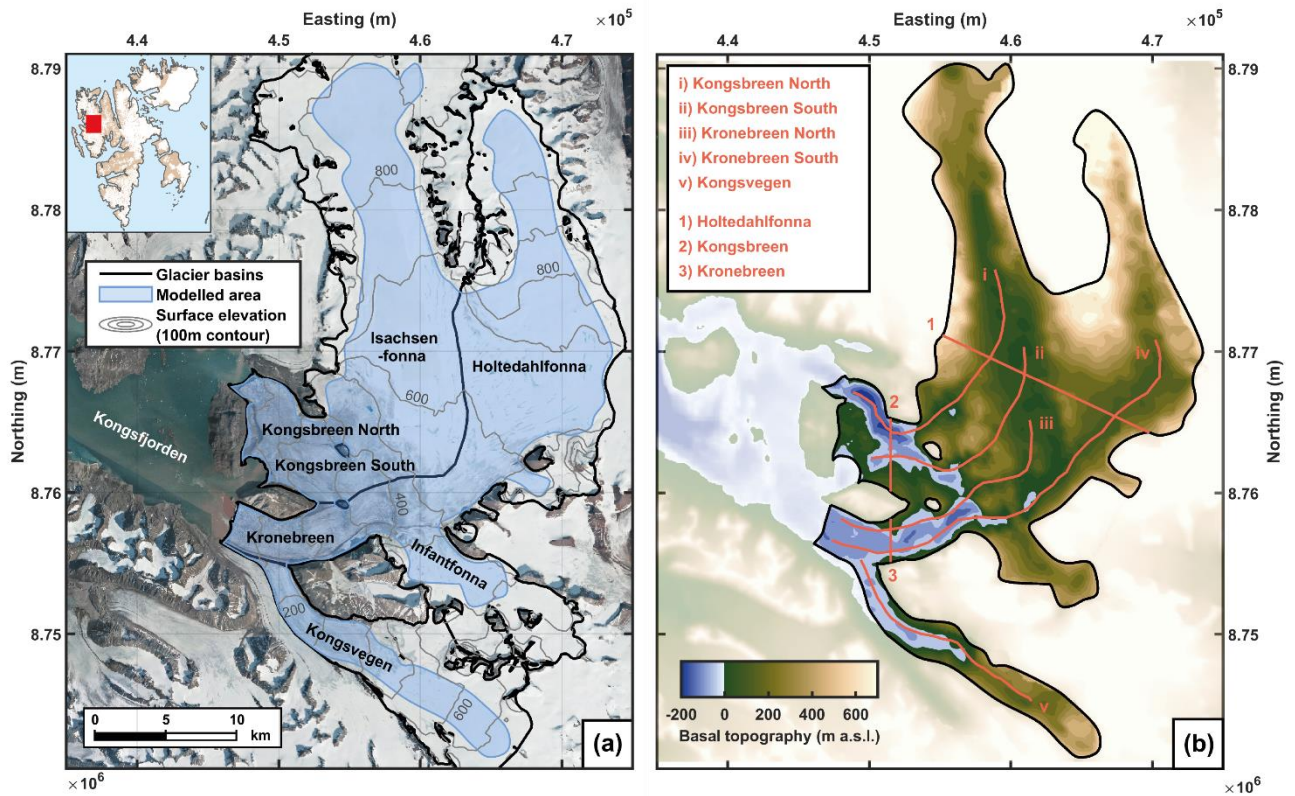
Figure 1. Kongsfjord basin with black line outlining the model domain. **(a)** Surface topography (Lindbäck et al., 2018) (background image: https://toposvalbard.npolar.no/, Norwegian Polar Institute), **(b)** Basal topography (Lindbäck et al., 2018) with (i–v) subglacial flowlines and (1–3) cross-glacier transects defined for analysing the model outputs.
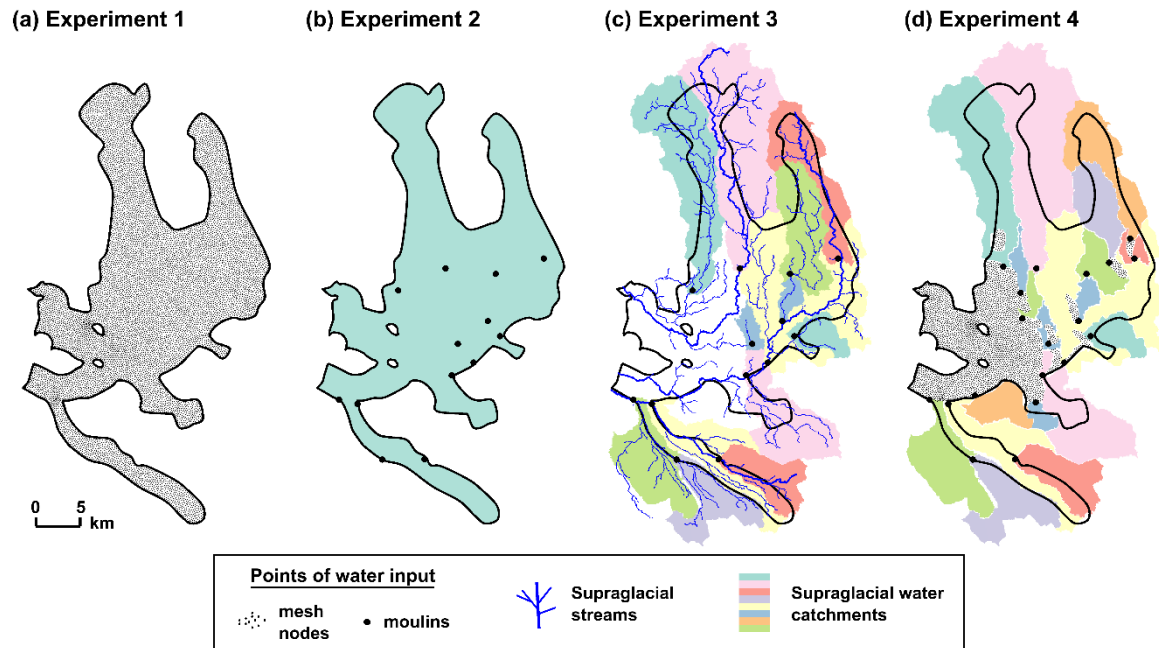
870

Figure 2. Water input distribution at the Kongsfjord basin for each experiment. Shown in black are the points of water recharge to the subglacial hydrological system, i.e. mesh nodes for **(a, d)** and moulins for **(b–d)**. The coloured areas are the supraglacial water catchments associated to the moulins. Subplot **(c)** also shows the TopoToolbox generated supraglacial stream network in blue.
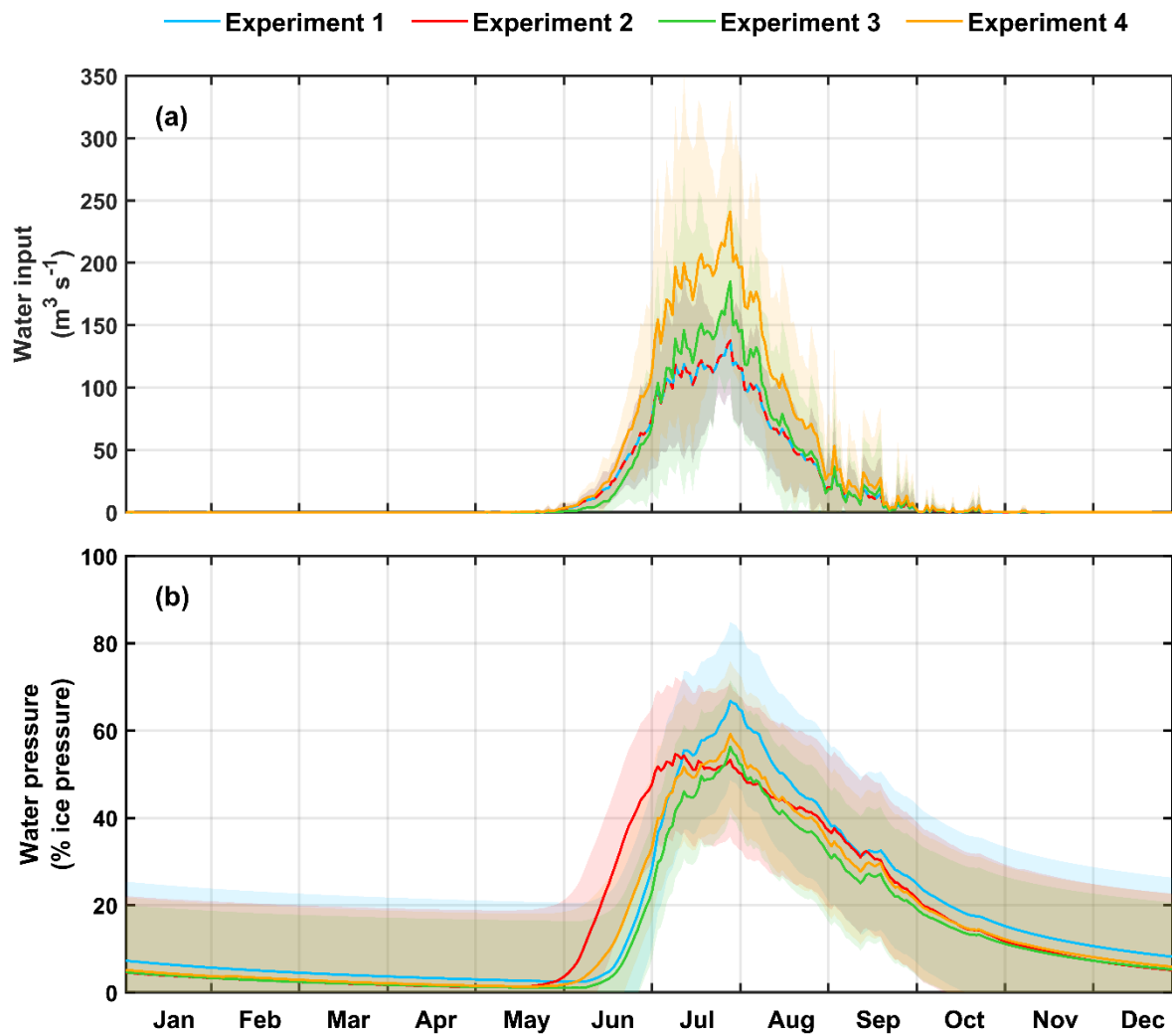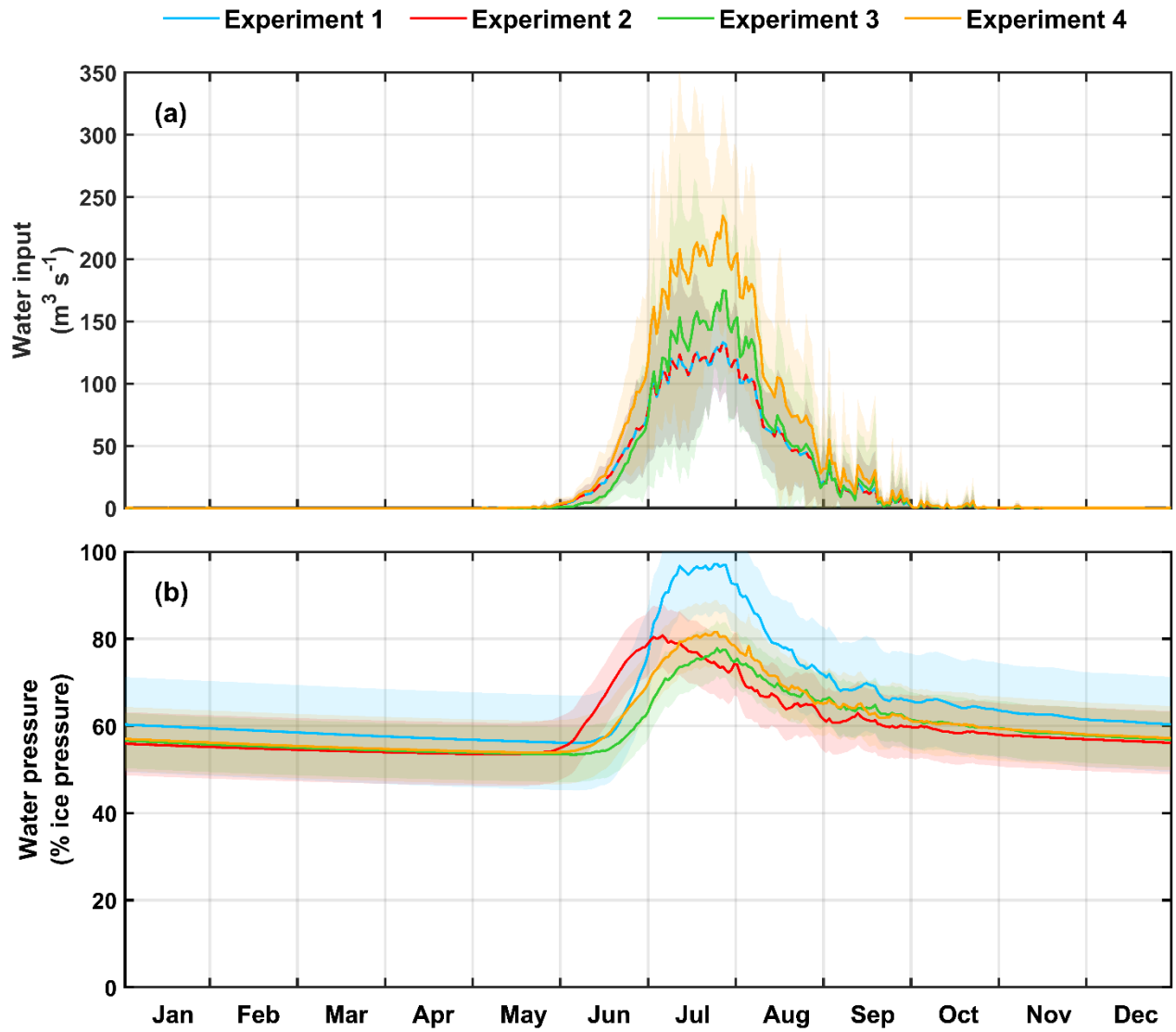
Figure 3. Mean (2004̶3–2017) annual **(a)** water input and **(b)** basal water pressure averaged over the whole model domain for each experiment. The shaded area is the standard deviation showing the interannual variability of water input and water pressure for each experiment.

880

Experiment 1   **Experiment 2 — Experiment 1**   **Experiment 3 — Experiment 1**   **Experiment 4 — Experiment 1**

(a) (b) (c) (d) April

(e) (f) (g) (h) June

(i) (j) (k) (l) July

0 5 km

0 20 40 60 80 100
Water pressure
(% ice pressure)

-20 -10 0 10 20
Water pressure bias
(% ice pressure)
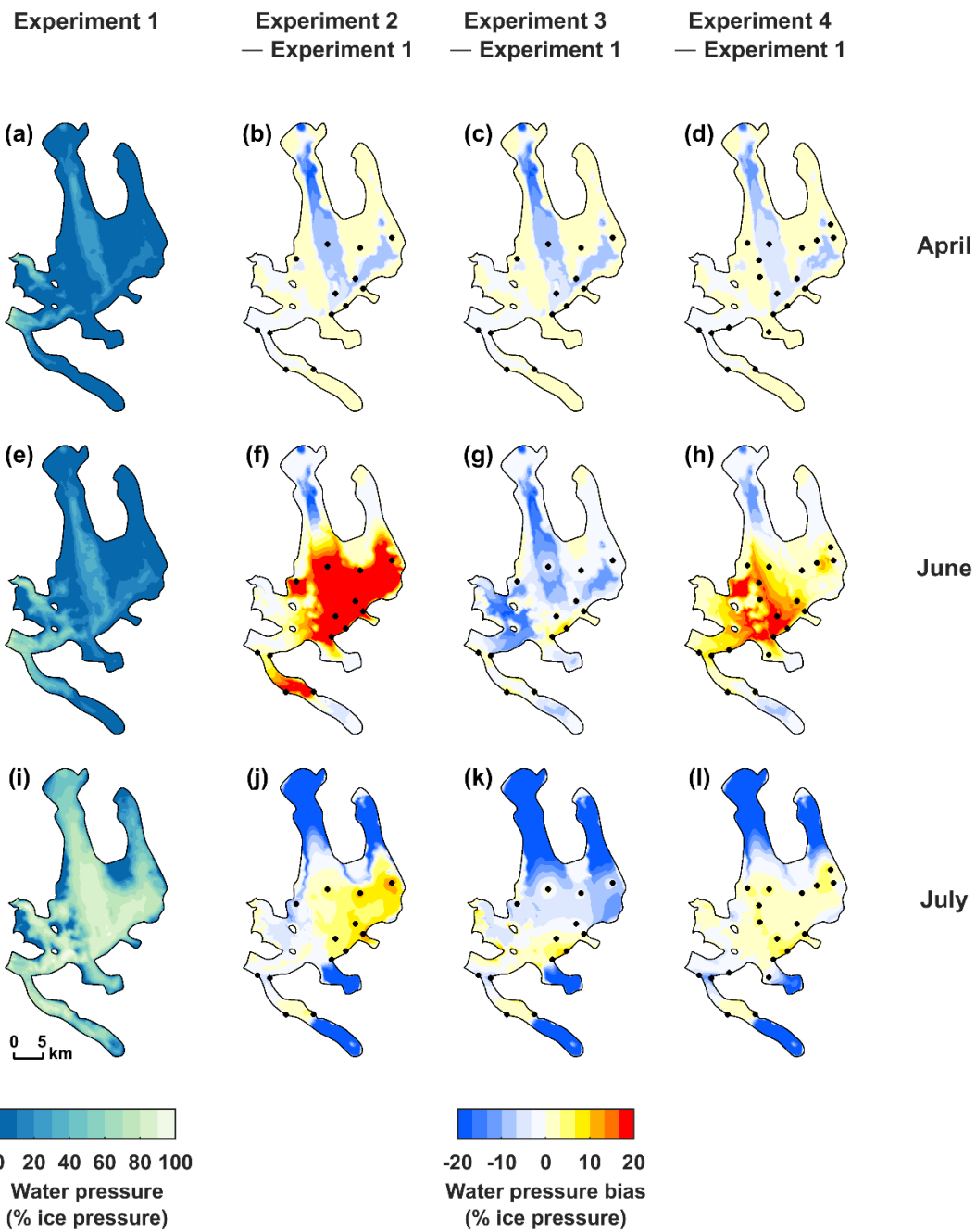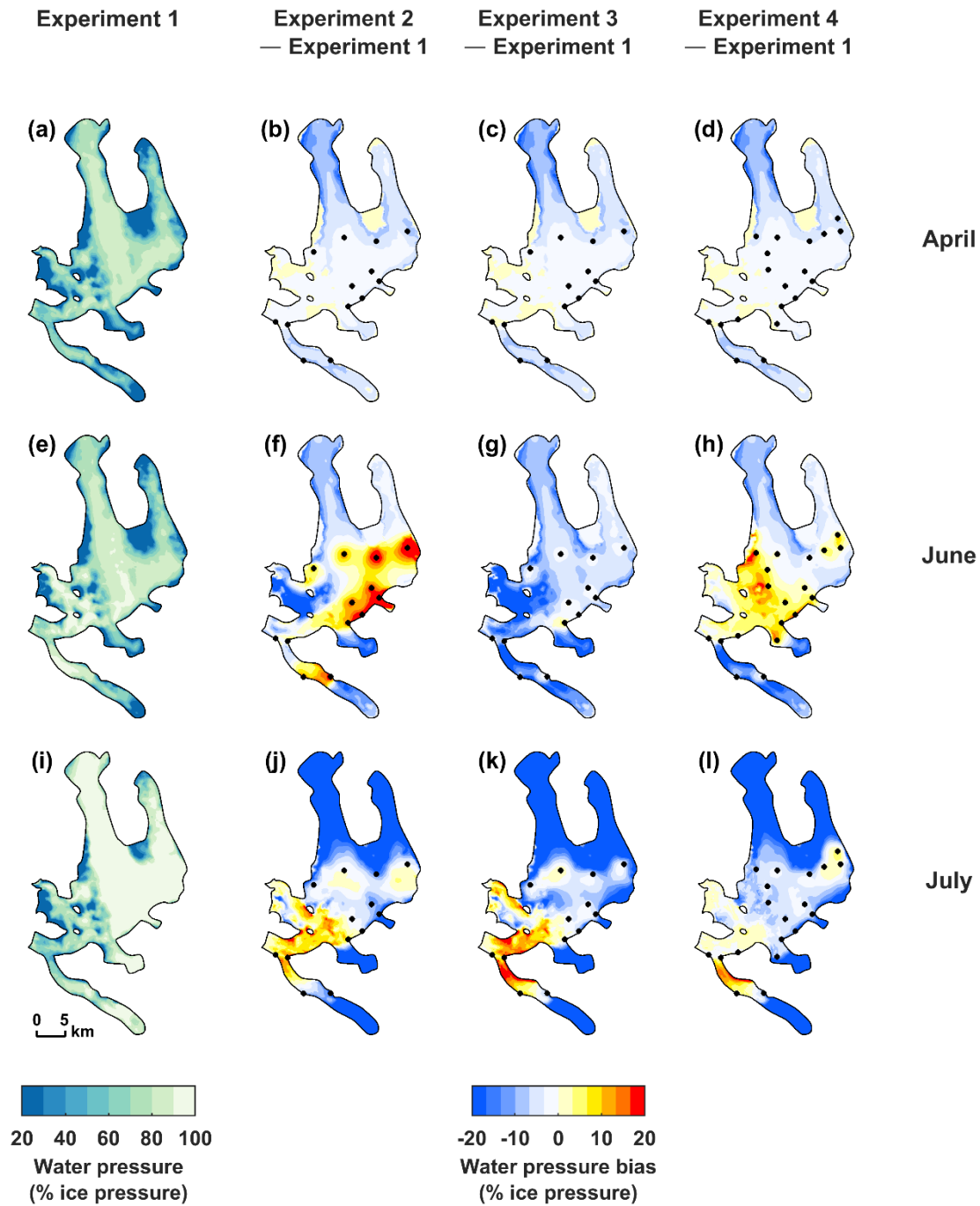
Figure 4. Mean (2004̶3̶–2017) basal water pressure modelled by Experiment 1 in **(a)** late winter (April), **(e)** early summer (June), and **(i)** mid-summer (July). Biases (differences to reference Experiment 1) in mean (2004̶3̶–2017) basal water pressure in **(b,c,d)** late winter

885   (April), **(f,g,h)** early summer (June), and **(j,k,l)** mid-summer (July). Basal water pressure is expressed as a fraction of the ice overburden pressure. The black dots mark the moulin locations.
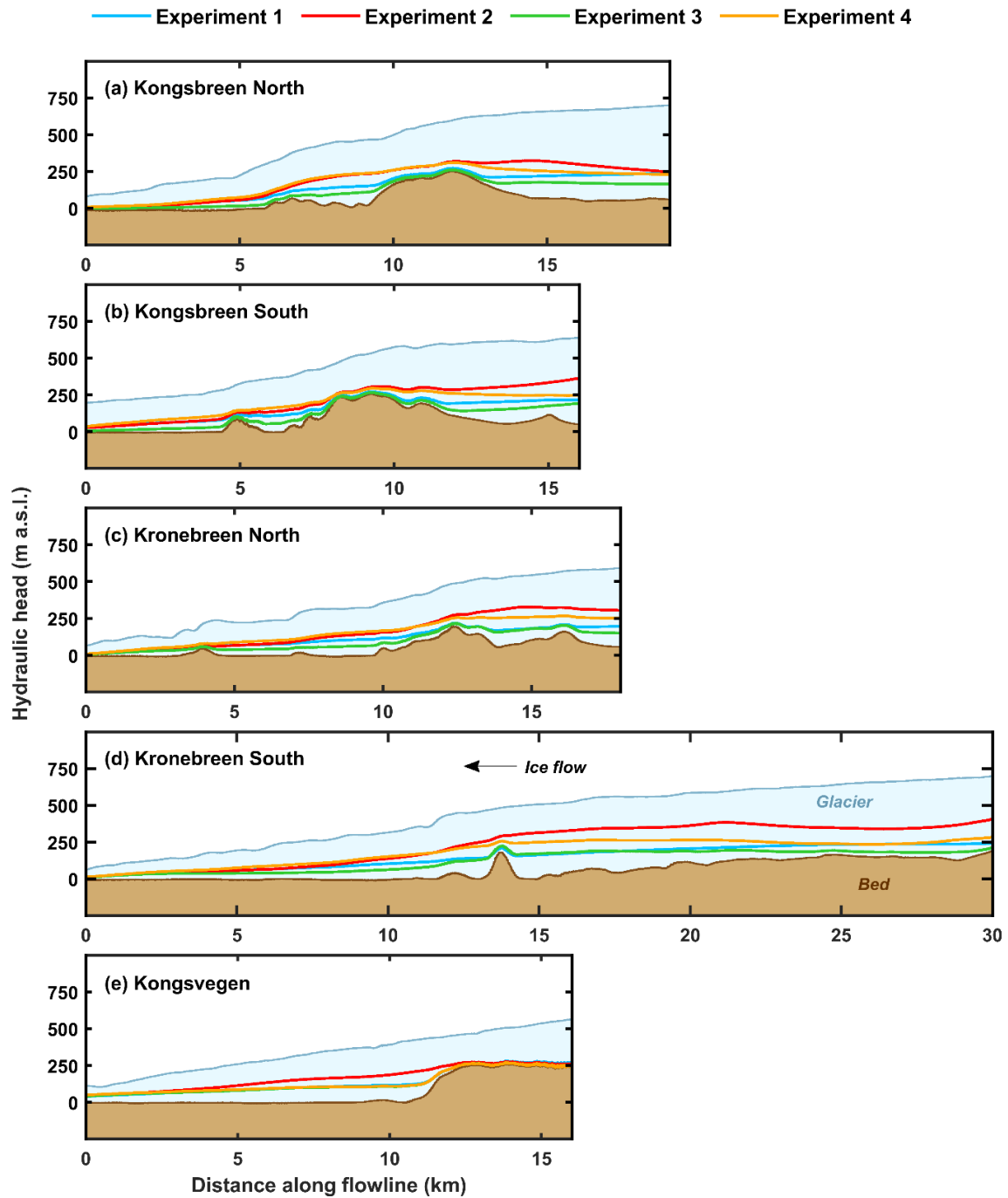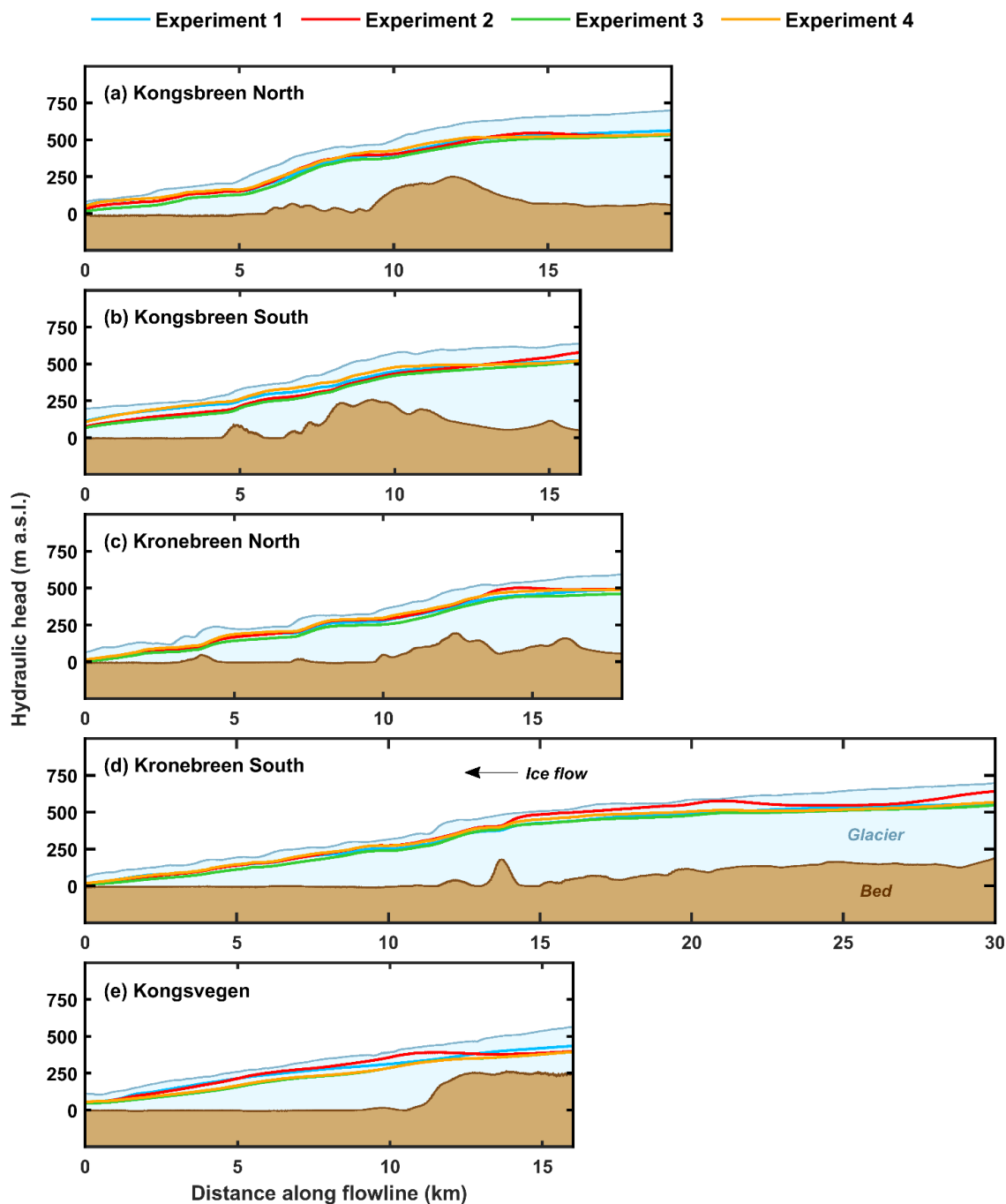
Figure 5. Mean (20043–2017) early melt season (June) hydraulic head modelled by each experiment at **(a)** Kongsbreen North, **(b)** Kongsbreen South, **(c)** Kronebreen North, **(d)** Kronebreen South, and **(e)** Kongsvegen. Hydraulic head is expressed in absolute values (m a.s.l.). Flowlines locations are shown in Fig. 1(b).

890

895
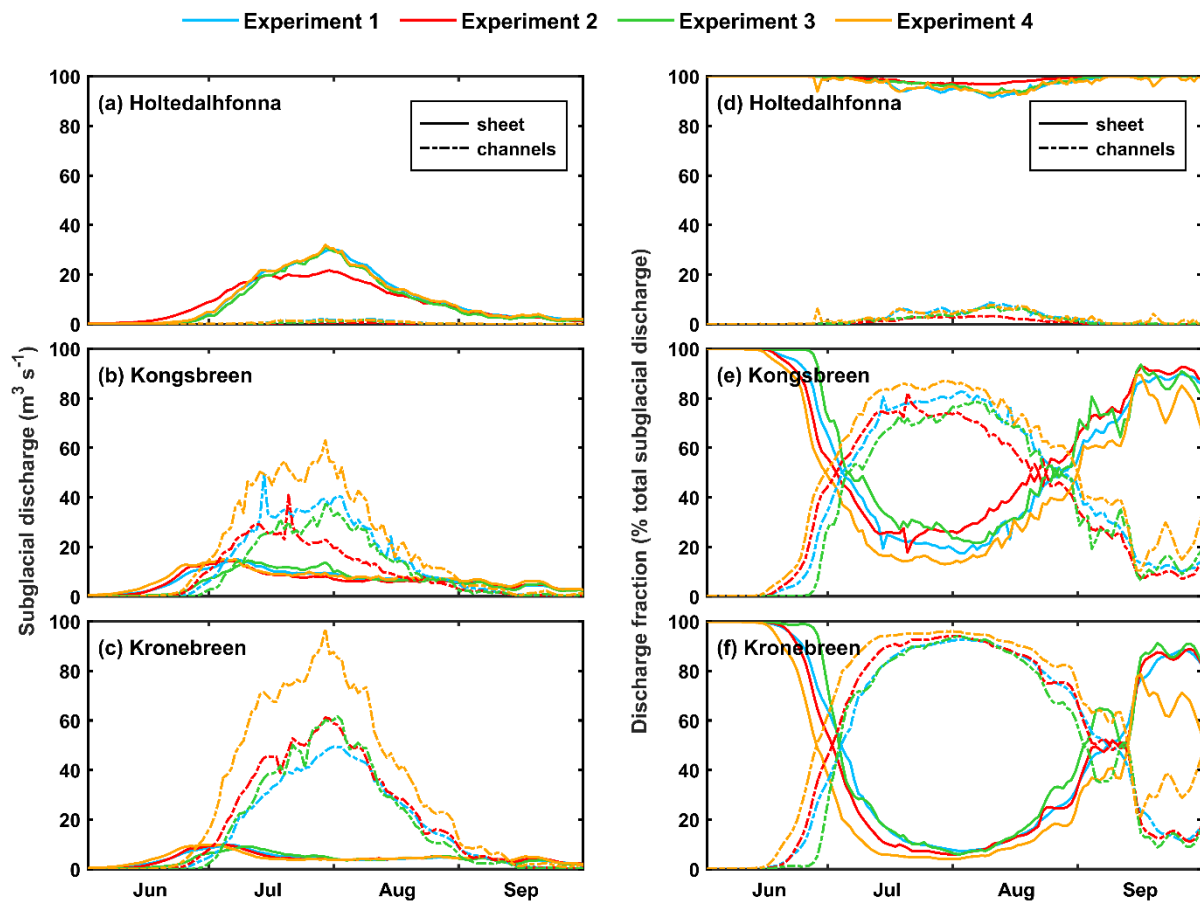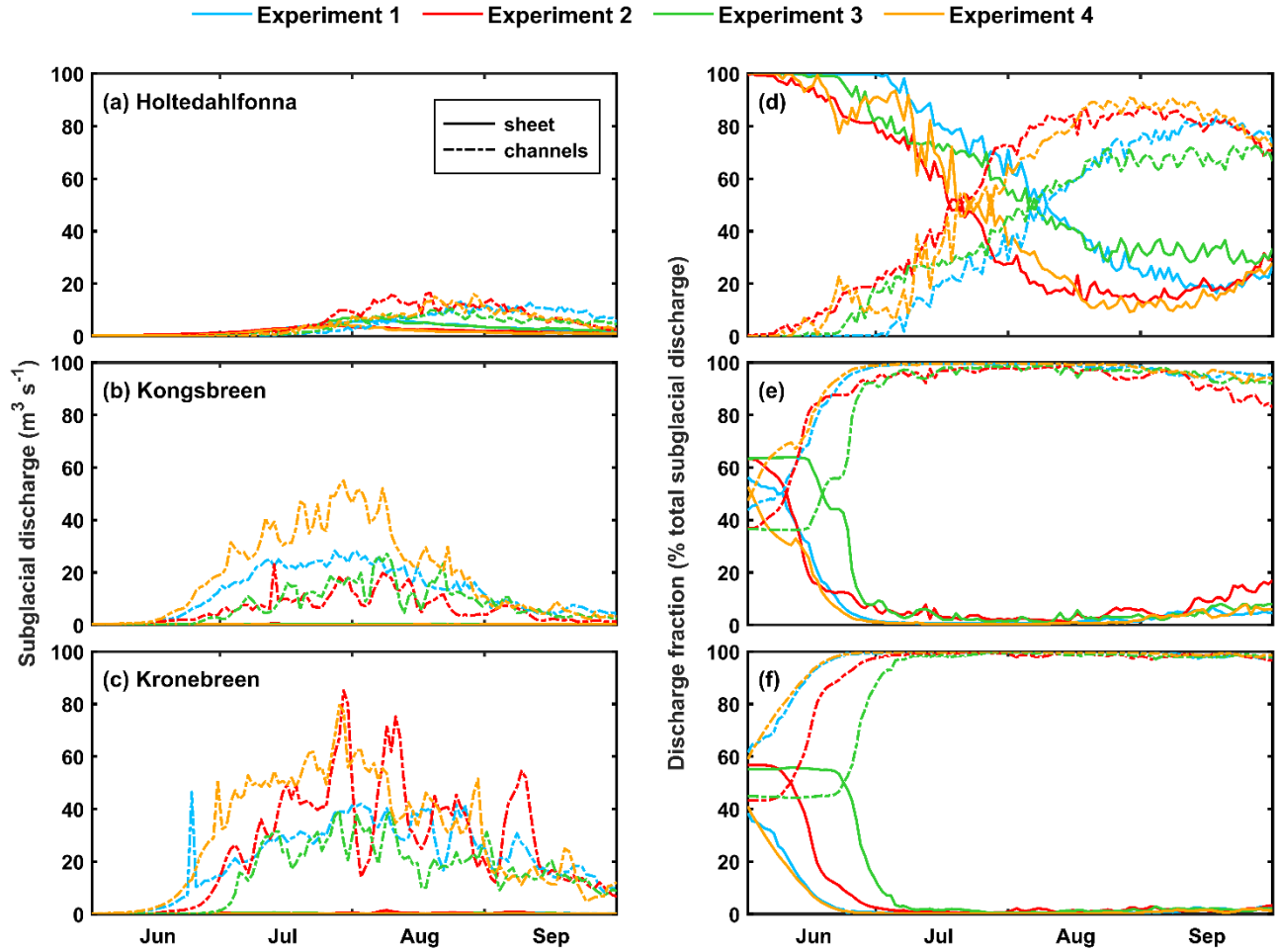
Figure 6. Left panel: Mean (20043–2017) summertime (June–September) sheet discharge and channel discharge modelled by each experiment across **(a)** Holtedahlfonna, **(b)** Kongsbreen and **(c)** Kronebreen. Sheet discharge is the cross-glacier width integral of the x component of the nodal sheet discharge. Channel discharge is the sum of discharge from all channel edges intersecting the cross-glacier section. Discharge is expressed in absolute values (m^3 s^{-1}). **Right panel:** Mean (20043–2017) summertime (June–September) sheet discharge and channel discharge modelled by each experiment across **(d)** Holtedahlfonna, **(e)** Kongsbreen and **(f)** Kronebreen. Here, discharge in the sheet and in the channels is expressed as a fraction of the total discharge (the sum of the discharge in the sheet and in the channels). Cross-glacier transects locations are shown in Fig. 1(b).
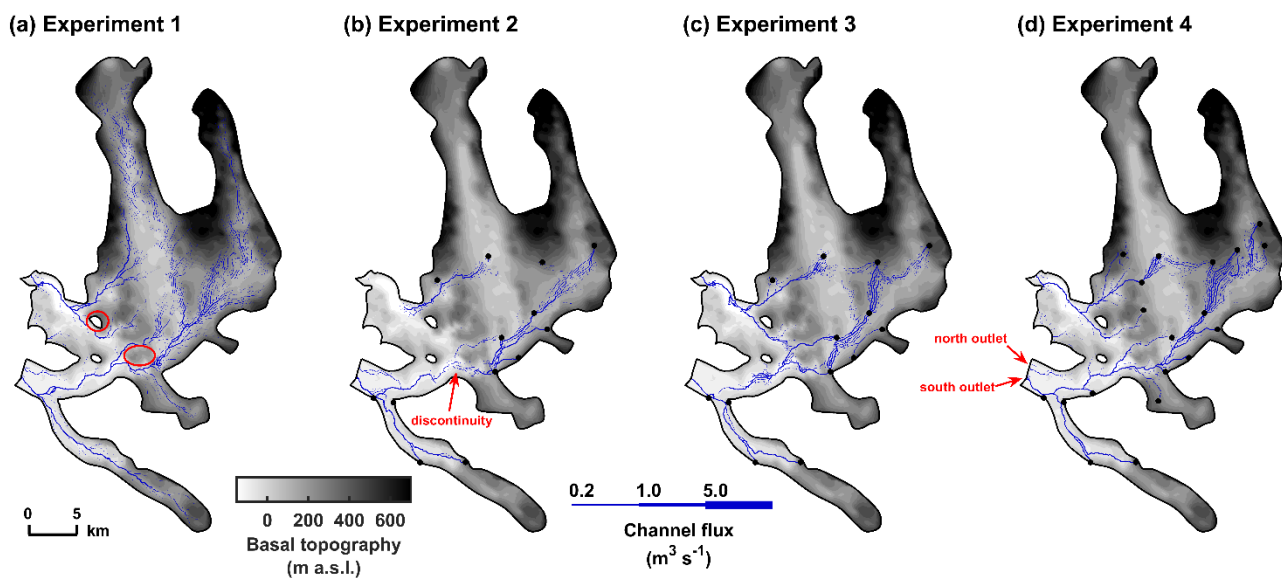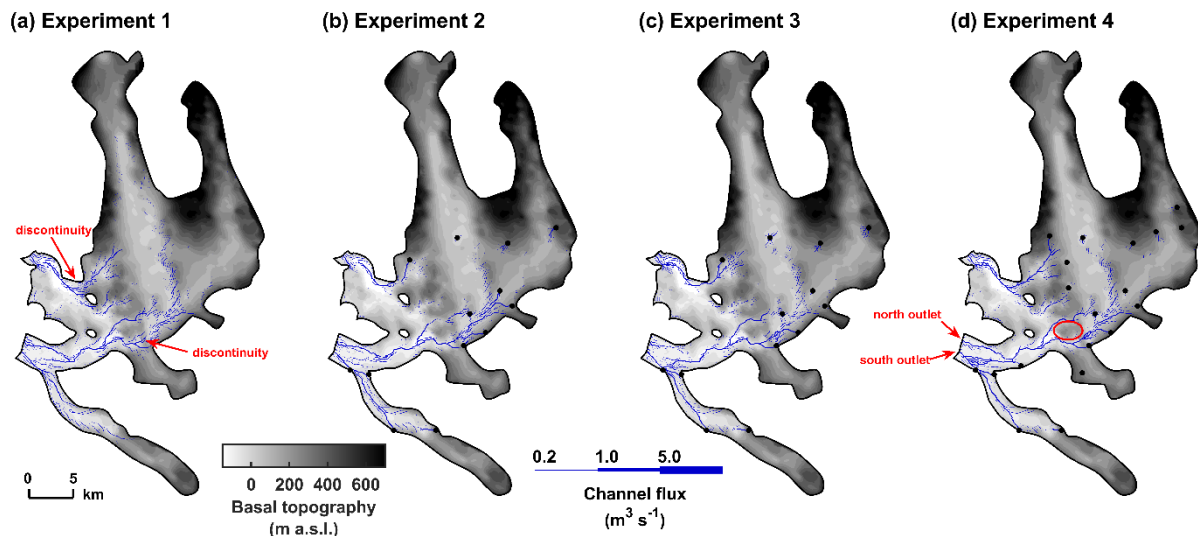
Figure 7. Summer snapshot (20th of August 2013) of subglacial channels distribution modelled by each experiment, with subglacial topography in greyscale. The year (2013) is chosen arbitrarily but is representative of the entire period. We use 1 m³ s⁻¹ as an arbitrary threshold flux to discriminate regions of significant channel size. ~~Discontinuities in the channel network due to basal adverse slopes are marked in red in Experiment 1 (a).~~ Nunatak and b~~B~~edrock spur splitting subglacial channels are~~is~~ circled in Experiment 1 (a).~~and f~~ Discontinuity in the channel network due to basal adverse slopes is marked in red in Experiment 2 (b). F~~f~~rontal outlets to subglacial runoff at Kronebreen/Kongsvegen are marked in red in Experiment 4 (**d**). The black dots mark the moulin locations.

(a) June   **(b) July**   **(c) August**

0   5
km

0 20 40 60 80 100
Water pressure
(% ice pressure)

0.2   1.0   5.0
Channel flux
(m^3 s^{-1})

920
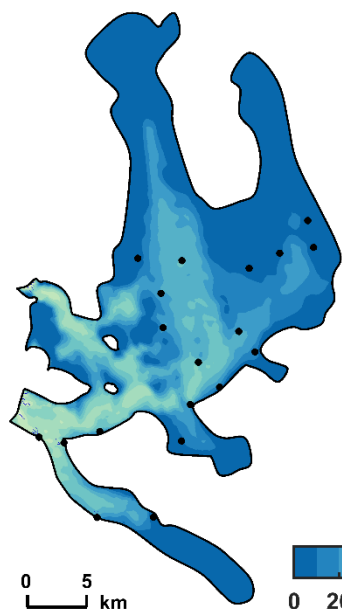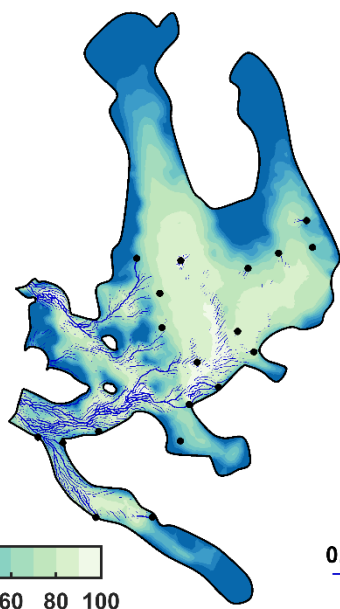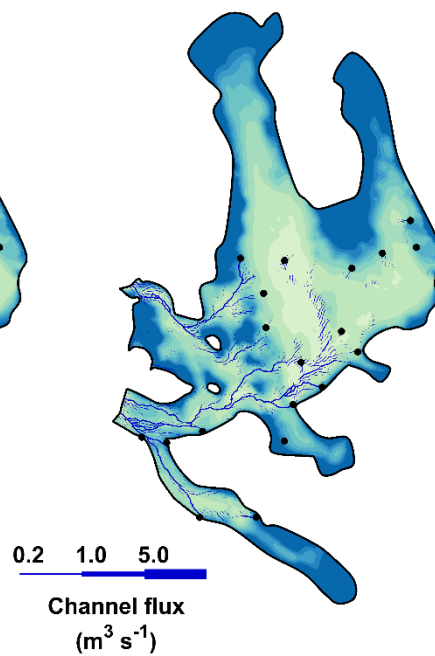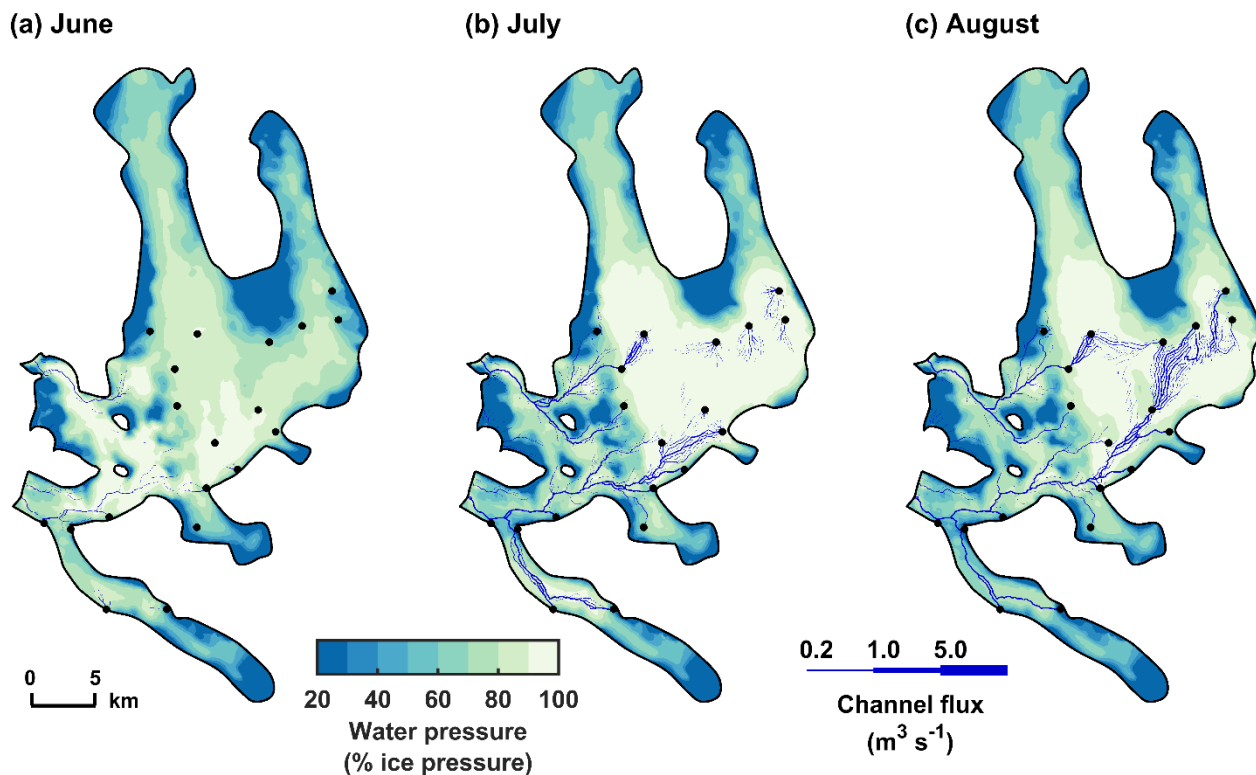
Figure 8. Mean (20043–2017) basal water pressure and channel discharge modelled by Experiment 4 in **(a)** early summer (June), **(b)** mid-summer (July), and **(c)** late summer (August). Snapshots of channel discharge are taken on (a) the 20th of June 2013, (b) the 20th of July 2013, and (c) the 20th of August 2013. The year (2013) is chosen arbitrarily but is representative of the entire period. Basal water pressure is expressed as a fraction of the ice overburden pressure. We use 1 m³ s⁻¹ as an arbitrary threshold flux to discriminate regions of significant channel size. The black dots mark the moulins locations.
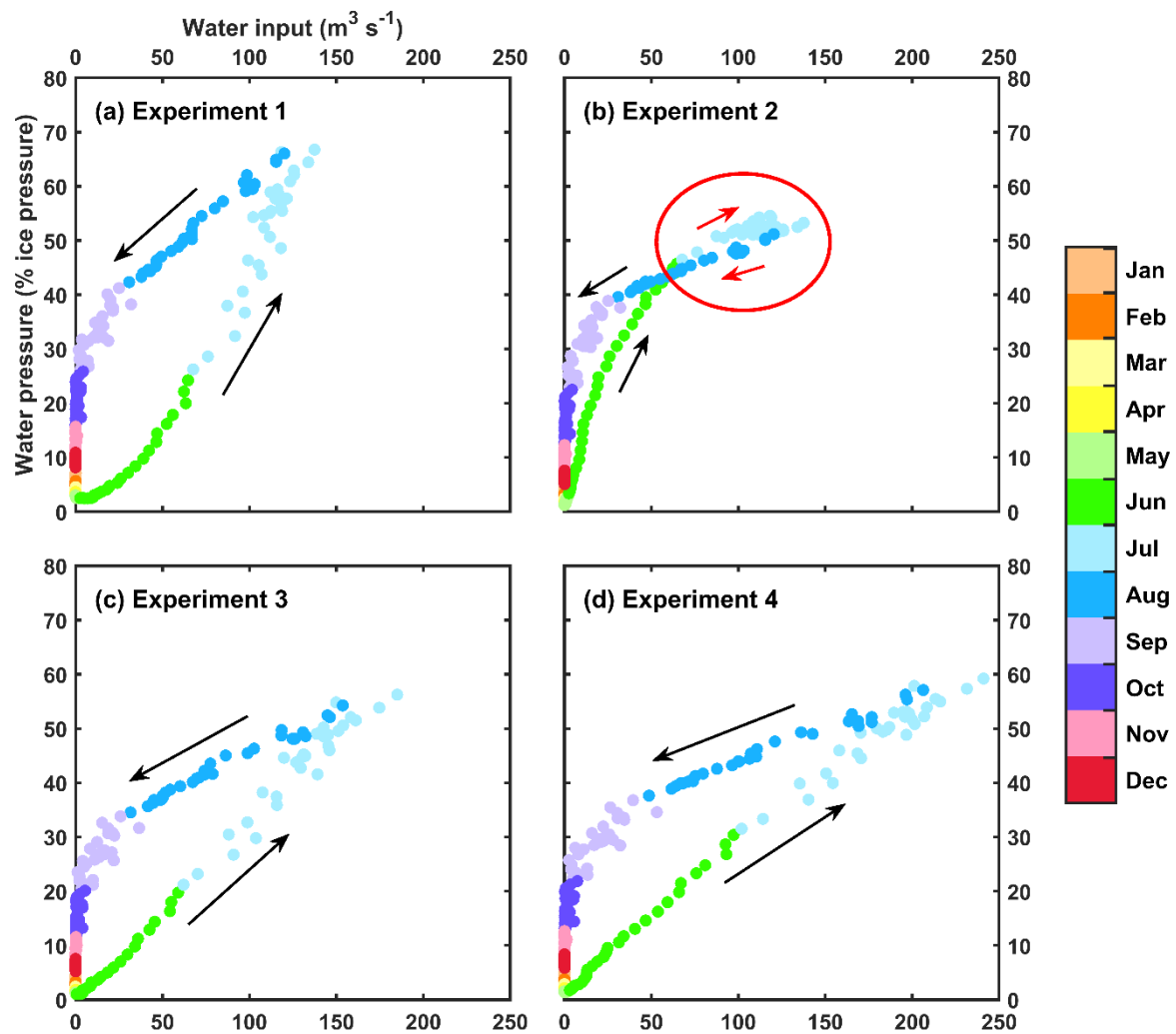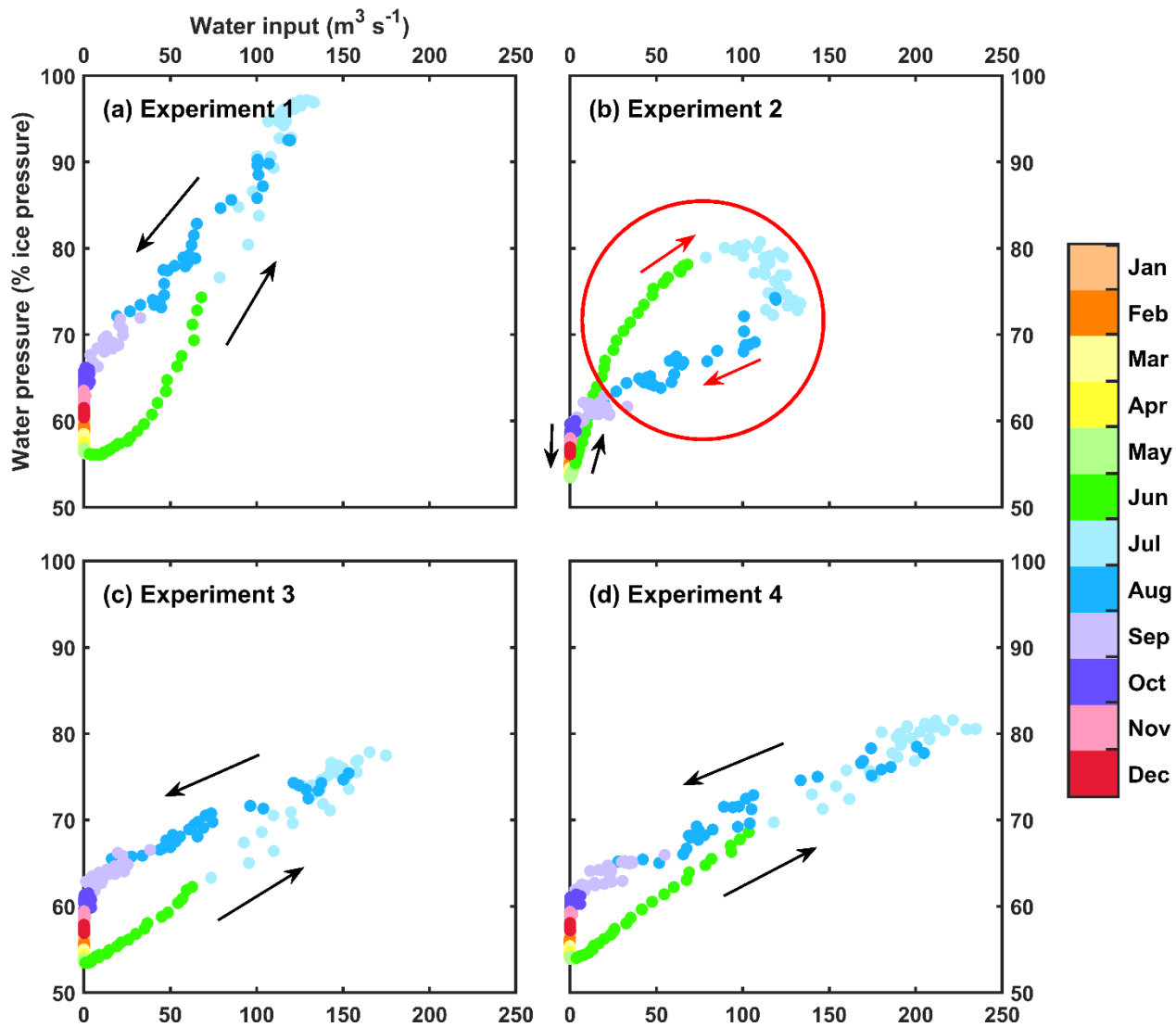
Figure 9. Relationship between water input and basal water pressure averaged over the whole model domain for each experiment during the mean (20~~43~~–2017) annual period. Clockwise hysteresis loop in Experiment 2 (b) between ~~late~~ mid-June and early September ~~mid-August~~ is marked in red. Water pressure is expressed as a fraction of the ice overburden pressure (%).

Description	Symbol	Value	Literature value	Units
Pressure melt coefficient	c_t	7.5×10^{-8}	7.5×10^{-8}	K Pa^{-1}
Heat capacity of water	c_w	4,220	4,220	J kg^{-1} K^{-1}
First sheet flow exponent	α_s	5/4	5/4	-
Second sheet flow exponent	β_s	3/2	3/2	-
First channel flow exponent	α_c	5/4	5/4	-
Second channel flow exponent	β_c	3/2	3/2	-
Sheet conductivity	k_s	10^{-4} ~~0.005~~	0.01	m$^{7/4}$ kg$^{-1/2}$
Channel conductivity	k_c	0.5	0.1	m$^{3/2}$ kg$^{-1/2}$
Ice flow constant cavities	A_s	6.8×10^{-24}	6.8×10^{-24}	Pa^{-3} s^{-1}
Ice flow constant channels	A_c	6.8×10^{-24}	6.8×10^{-24}	Pa^{-3} s^{-1}
Sheet width below channel	l_c	5	2	m
Cavity spacing	l_r	2	2	m
Bedrock bump height	h_r	0.1	0.1	m
Englacial void ratio	e_v	10^{-4}	10^{-4}	-
Moulin cross-sectional area	A_m	4	4	m^2
Basal sliding speed	u_b	10^{-5}	10^{-6}	m s^{-1}

Table 1. Parameters and values used in GlaDS for all model runs in this study. Grey highlighted parameter values are those that are not taken from literature. Literature values are taken from Werder et al. (2013).

940